SPECTRAL SUB-BAND SYNTHESIS USING MULTIPLE INDEPENDENT LASERS AND RECEIVER DSP FOR HIGH BAUD-RATE SINGLE-CARRIER Tb/s TRANSMISSIONS

YIN TAT WONG

MPhil

The Hong Kong Polytechnic University

2018

The Hong Kong Polytechnic University

Department of Electrical Engineering

SPECTRAL SUB-BAND SYNTHESIS USING MULTIPLE INDEPENDENT LASERS AND RECEIVER DSP FOR HIGH BAUD-RATE SINGLE-CARRIER Tb/s TRANSMISSIONS

YIN TAT WONG

A thesis submitted in partial fulfillment of the requirements for the degree of Master of Philosophy

March 2018

Certificate of Originality

I hereby declare that this thesis is my own work and that, to the best of my knowledge and belief, it reproduces no material previously published or written, nor material that has been accepted for the award of any other degree or diploma, except where due acknowledgement has been made in the text.

………………………………………….. (Signed)

WONG YIN TAT
………………………………………….. (Name of student)

Abstract

In recent years, the ever-emerging internet application has driven the development of optical communication capacities. Other than meeting the current demand, the increment of capacity will enable various applications which could be or could not be imagined, including remote diagnosis and remote surgery.

To achieve this goal, effort needed to be made on both transmitter and receiver side. On the transmitter side, most of the proposed spectral slicing transmitters in previous journals included a key component named frequency comb generator, which generates a series of carriers with different frequency by a single monochromatic laser. The generated carriers will then be modulated separately and multiplexed at transmitter output. Owing to the characteristics of frequency comb generator, frequency as well as phase of carriers were locked, thus larger bandwidth signal could be generated at ease.

We are proposing a different transmitter architecture, which replaced the monochromatic laser and frequency comb generator with multiple sets of monochromatic lasers, aiming to improve the flexibility achieving single carrier transmission. However, given frequencies and phases of lasers were not locked in the proposed setup, new symbol distortion was found in the research progress and was discussed in this thesis.

To overcome distortion brought by the proposed transmitter, we also proposed a digital signal processing (DSP) platform, which consists of modified frequency offset estimation algorithm, conventional CMA, and BPS at the receiver. Simulation result showed a transmission rate of 1 Tb/s could be achieved with PM-16-QAM format and 4 lasers.

Acknowledgements

I would like to express my gratitude to my supervisor, Dr. Alan Pak Tao Lau, for his professional knowledge and unlimited support. Other than completing the thesis, he also enlightened me the way of thinking, how to raise a question, and pointed out the importance of developing personal skill set. I would not be able to complete this thesis without his guidance and support.

Also, I would like to appreciate the help from my ex-colleague Elwin Ha, for introducing the basics of optical communication and showed the attitude to research. The research progress would not be so smooth without his patience and assistance.

Table of Contents

List of Abbreviations

ABI - Analog Band Interleaving
ASE - Amplified Spontaneous Emission
AWGN - Additive White Gaussian Noise

BER - Bit Error Rate
BPS - Blind Phase Searching

CD - Chromatic Dispersion
CFO – Carrier Frequency Offset
CMA - Constant Modulus Algorithm
CPE - Carrier Phase Estimation
CRLB - Cramer - Rao Lower Bound
CW - Continuous Wave

DA – Data Aided
DAC - Digital to Analog Converters
DBI - Analog Band Interleaving
DFT - Discrete Fourier Transform
DSP - Digital Signal Processing
DWDM - Dense Wavelength Division Multiplexing

ECL - External Cavity Lasers
EDFA - Erbium Doped Fiber Amplifier
EKL – Extended Kalman Filter
ETDM - Electronic Time Division Multiplexing
E/O - Electro - Optic
EVM - Error Vector Magnitude

FFT - Fast Fourier Transform
FO - Frequency Offset
FOC – Frequency Offset Compensation
FOE - Frequency Offset Estimation (algorithm)

ICI - Inter Carrier Interference
IMDD - Intensity Modulation, Direct Detection
InP - Indium - Phosphide
ISI - Inter Symbol Interference

LiNbO3 - Lithium Niobate
LMS - Least Mean Square
LPN - Laser Phase Noise
LTI – Linear, Time Invariant

MIMO – Multiple Input, Multiple Output
ML - Maximum Likelihood

MZM - Mach - Zehnder Modulator

NDA – Non-Data Aided

OFCG - Optical Frequency Comb Generator
OSNR – Optical Signal to Noise Ratio
OTDM - Optical Time Division Multiplexing

PLL - Phase Lock Loop
PMD - Polarization Mode Dispersion
PRBS – Pseudo Random Bit Sequence
PSK – Phase Shift Keying

QAM - Quadrature - amplitude Modulation
QPSK - Quadrature Phase Shift Keying

RLS - Recursive Least Squares

SDN - Software Defined Network
SE - Spectral Efficiency
SNR – Signal to Noise Ratio

TDM - Time Division Multiplexing

VVPE – Viterbi-Viterbi Phase Estimation

WDM – Wavelength Division Multiplexing

Chapter 1

Introduction

1.1 Motivation of the thesis

Considerable growth in Fiber-optic communications throughout the last decade was mainly driven by consistently increasing needs for higher transmission rate, where such trend is growing exponentially. Carrying capacity of optical communication system has been increased by approximately 10000 times, while traffic load only increased by 100 times over past 30 years. However, another growth factor of 100 was predicted within 10 years [1]. Besides load of traffic, increasing trend of number of users and averaged bandwidth consumed were noticeable as well.

To satisfy the future needs of Internet traffic, Coherent optical fiber communication was developed comprehensively in the 80s due to sensitivity in receivers [2]. However, the emergence of wavelength-division multiplexed system (WDM), erbium-doped fiber amplifier (EDFA) together with intensity-modulation, direct detection (IMDD) once became researchers' controversial issue, by enabling higher capacity, transmission distance with loss compensated by EDFAs [3]. Carrier phase estimation algorithm proposed in 2005 made Coherent optical communication comparable to WDM system, as modulation format with higher spectral efficiency (SE), such as quadrature-amplitude modulation (QAM), could be introduced to coherent optical communication system [4].

Development of high speed digital to analog converter (DAC), which fueled by the demand towards high bandwidth internet traffic recently, has improved the overall symbol rate dramatically. However, as stated in [1], internet traffic is expected to grow by a factor of 10 within this decade and corresponding DAC development are still inadequate to fulfill the trend. Achieving high symbol rate single carrier signals for Tb/s transmission is currently one of the recent research interest. As development of bandwidth provided by DAC is slow, relatively to the increasing needs for internet traffic, providing high bandwidth transmission simply by developing high speed DAC is unpractical. Introduction of multiplexing technique ease the harsh bandwidth demand for DAC and achieving high overall line rate meanwhile.

Digital signal processing (DSP) also played a major role throughout the development of coherent optical transmission system. By compensating various non-idealities throughout the channel, sophisticated and advance modulation formats were attractive for next generation communication system as higher degree of freedom, including space, time, frequency, polarization and phase [5] [6], were ready to be exploited for encoding data, or used for estimation to compensate channel impairments on the other hand. Both approach will eventually improve channel capacity and spectral efficiency (SE) of fiber channels.

Other than multiplexing technique, which aimed to provide high bandwidth transmission through working in time domain, another class of approach called spectral stitching achieve the same goal via processing in frequency domain. Frequency comb generator acted as a key system component where single laser input was split down to multiple carriers with their corresponding phase and frequency locked, where the locking property is crucial to minimize inter-channel carrier interference (ICI). However, several proposed architectures were still not attractive and not commercially available for practical implementation.

Hence, we are proposing a transmitter architecture achieving high bandwidth transmission, by replacing the frequency comb generator to multiple independent lasers, with a modified DSP algorithm in the receiver. The proposed configuration enables flexible transmissions of spectral slicing super-channels and conventional WDM signals, is valuable for future software-defined transmissions, where both high channel capacity and flexibility is required.

1.2 Development in high bandwidth transmission

1.2.1 Digital to analog converter (DAC)

Rising needs for internet traffic leading to increasing demand for high bandwidth transmission in near future, where 100Gb/s class optical data carrying components have been examined extensively [7] [8] [9] [10], where achieving high baud-rate is primary approach to accommodate this. Among different opto-electronics components, digital to analog converters (DAC) and analog to digital converters (ADC) are critical components that hindered the overall development. Among DAC and ADC, bandwidth provided by DAC is crucial as bandwidth narrowing that occurred in transmitter end will deteriorate overall signal quality.

1.2.2 Time division multiplexing (TDM)

An independent DAC provide acceptable bandwidth for general usage, but not for high bandwidth transmission. Employing 6 bits, a SiGe DAC could achieve 100GSa/s sampling rate, with 40GHz 3 dB bandwidth [11]. Thus, multiplexing techniques, by means of electronic or optical domain, were widely applied in DAC structure to generate higher symbol rate. Using electronic time division multiplexing (ETDM) among SiGe DACs, transmission of 72GBd 64-QAM signals was recorded [9]. Applying coarse bit resolution and combining DACs, line rate of 1.08Tb/s in a single carrier could also be achieved with 90GBd 64QAM signal [12]. Further higher symbol rate could be generated by multiplexing various binary DACs, for instance 120GBd 16-QAM and 138GBd QPSK signal [13] [14].

On the other hand, similar approach could be applied in optical domain to achieve optical time division multiplexing (OTDM) [15, 15] [16]. OTDM is still under development and not available in market yet, as more optical carriers and modulators were required, as well as precise phase matching to guarantee the quality of symbol constellation.

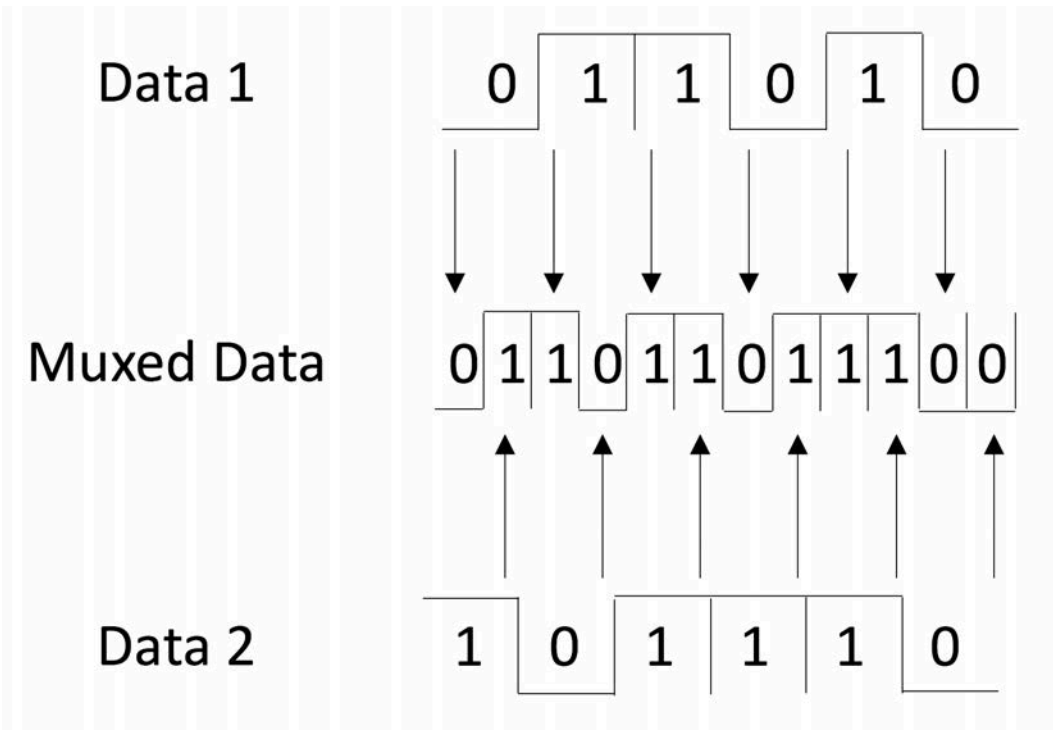

Fig. 1.1 Principle of TDM

1.2.3 Analog/Digital band interleaving (ABI/DBI)

Since numerous carriers and electro-optic modulators were required in OTDM, as well as additional precise time delay control loop at each input of multiplexer, analog/digital band interleaving (ABI/DBI) were proposed to generate larger bandwidth at DAC output, compared to TDM approaches.

Idea of ABI/DBI was proposed back in 2005 [17], which is a technique which combines spectra in electronic manner to form a large electronic spectrum. Exploiting multiple number of low bandwidth DACs, 100GBaud or even higher symbol rate can be generated [18] [19] [20].

Figure 1.2 showing block diagram of ABI/DBI technique. Sub-bands were separated in digital domain and passed to DACs, which were arranged in parallel manner and responsible for a fraction of the entire spectrum. Each sub-band's digital signal was first passed to low speed DAC and converted to analog signal of sub-bands respectively. An extra DAC was implemented to generate local oscillator with accurate frequency, which were used for mixing converted baseband analog signal to form sub-band signal with correct frequency. Edges of up converted sub-bands were trimmed with band pass filter of selected frequency and bandwidth, and eventually passed to mixer to generate a spectrum with large bandwidth.

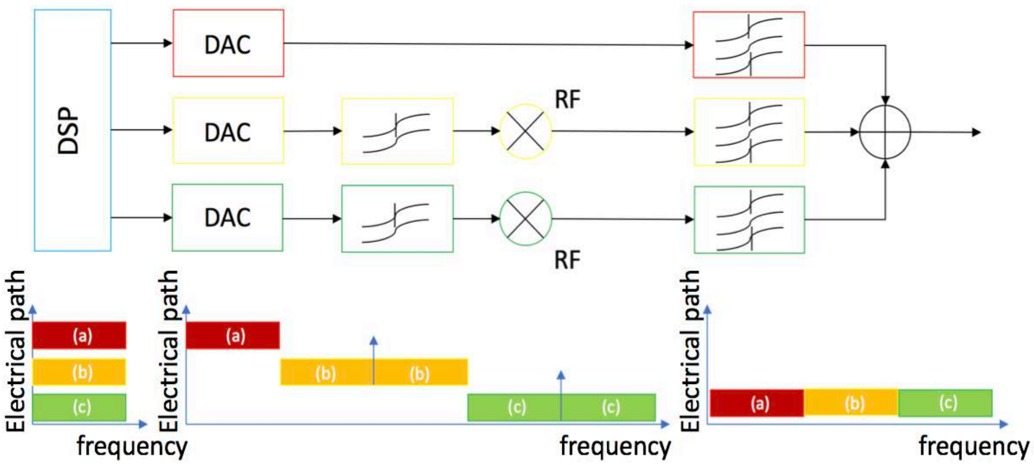

Fig. 1.2 Block diagram of ABI/DBI technique

1.3 Spectral slicing

1.3.1 Bottleneck met by ABI/DBI

With ABI/DBI technique, large bandwidth exceeds 100GHz can be generated within a DAC. Figure 1.3 showed a general structure of transmitter and showed the position of DAC. For general transmitter structure, a DAC is connected to a Mach-Zehnder Modulator (MZM), along with an external cavity laser (ECL), where signal output from DAC were modulated to designated format and carrier frequency, depends on structure of MZM and linewidth of ECL used, hence eliminated the requirement of frequency and time alignment and precise optical phase control to prevent any superposition occurred in separately modulated optical signals. However, to the best of our knowledge, there is no any individual modulator commercially available or even under development in the laboratory can support signal with bandwidth beyond 100GHz. For example, most of the Lithium Niobate ($LiNbO_3$) modulators which are commercially available, possess 3-dB electro-optic (E/O) bandwidth about 35GHz [21] [22]; Indium-phosphide (InP), polymer and electro-absorption modulators developed in laboratory barely meet the benchmark of 100GHz 3-dB E/O bandwidth [23] [24] [25]. Thus, spectral slicing technique, or spectral synthesis, were proposed to overcome this issue.

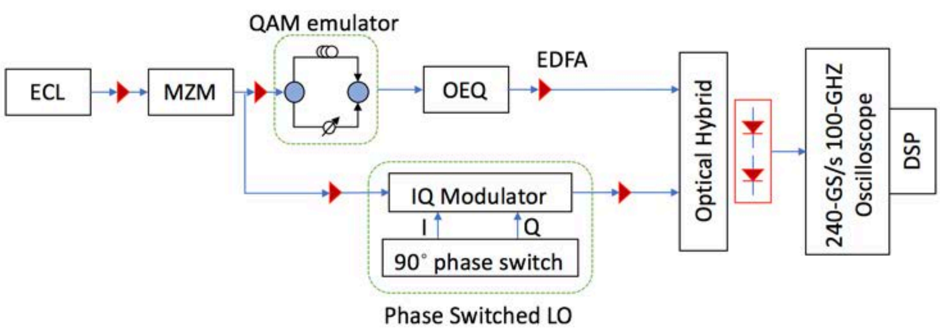

Fig. 1.3 General structure of transmitter with DAC employing ABI/DBI technique

1.3.2 Bottleneck met by TDM

Figure 1.4 showing the conversion of short pulse between time and Fourier domain. As observed, the shorter the pulse width in time domain, the wider bandwidth is required in frequency domain.

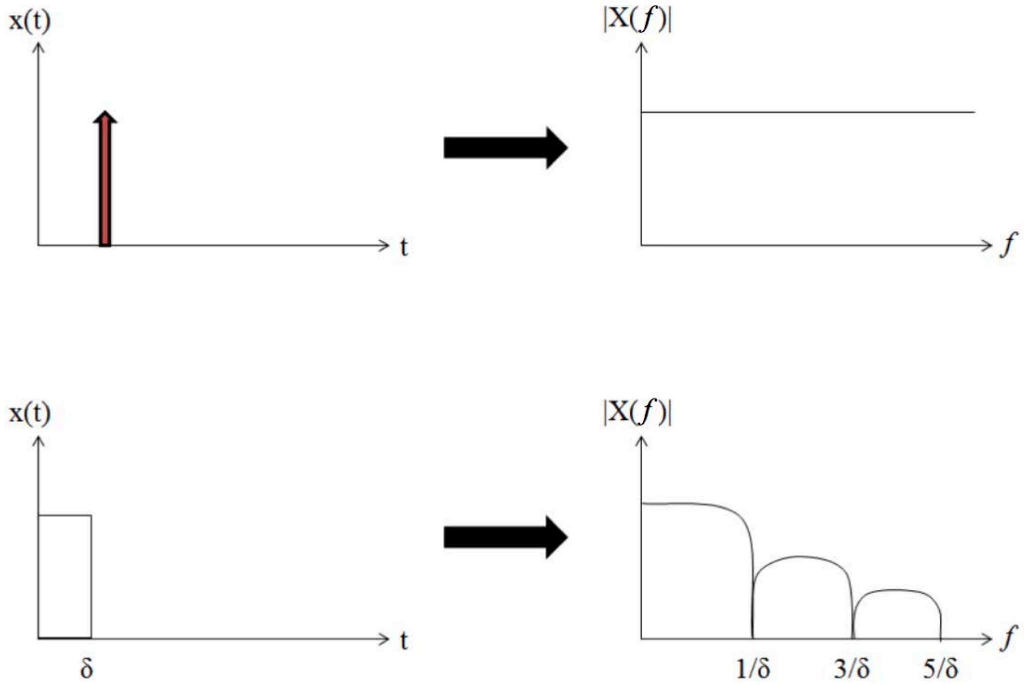

Fig. 1.4 Conversion of short pulse with pulse length δ between time and frequency domain

With high switching speed in a single DAC, high switching loss and other unwanted effect may become noticeable, which indirectly stated the bottleneck met by TDM approach development. Besides, TDM shared a similar drawback to ADI/DBI technique, which is their locality. Both techniques could manufacture DAC with bandwidth higher than 100GHz, but generated signal were restricted to be modulated by a single modulator for most of the time. Offline modifications will be required if data transmission rate demanded by client is changed, which limited the flexibility, one of the key component in next generation software defined network (SDN).

1.3.3 Principle of spectral slicing

Comparing to other ABI/DBI technique mentioned earlier, spectral slicing technique ease the need of ultra-high speed DAC and bandwidth requirement in other opto-electronic component such as modulators. A general setup of spectral sliced transmitter was shown in Fig. 1.5.

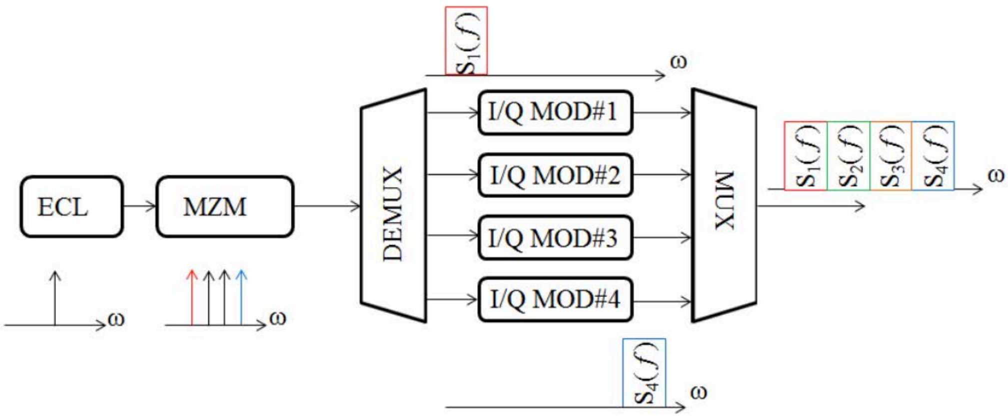

Fig. 1.5 Setup of spectral slice transmitter

Overall signal to be transmitted is preprocessed with Transmitter DSP and split into several parts, depends on number of sub-band is used to regenerate the entire signal. For example, 4 30GHz DACs and MZMs were used to reconstruct a signal with a bandwidth of 120GHz. Like ABI/DBI techniques, signal in DACs were treated as baseband signal and split into 4 sub-bands, hence lower speed DAC can be applied. Sliced sub-band signal from DACs output were passed to separate individual MZM modulators, where each of them will be modulated to correct carrier frequency. Modulated sub-bands went through corresponding delay line to maintain precise optical time alignment and eventually coupled to regenerate a signal of 120GHz overall bandwidth, from 4 30GHz DACs and separate modulators.

1.3.4 Principle, application and drawbacks of optical frequency comb generator (OFCG)

A set of ECL, MZM and de-multiplexer was shown in the Figure 1.5., which was known as optical frequency comb generator (OFCG), based on the teeth of comb waveform shown in the screen of spectral analyzer. Figure 1.6 showed the simplified block diagram of OFCG. The ECL was first injected into the optics box and phase modulated by the E/O phase modulator. Erbium doped fiber amplifier (EDFA) was applied within the optical loop to compensate insertion loss between components and guarantee high Q-factor throughout the process. After several circulations around the box, with amplifier and WDM coupler, a comb of frequency spikes was generated and could be found on the screen of optical spectral analyzer, an example is shown in Figure 1.7. Frequency spacing between carriers were determined by the effective length of fiber within the ring, which can be adjusted by the adjustable delay line. Theoretically, an OFCG can generate comb of carriers with various selected frequency spacing, with corresponding frequency and phase locked. Hence, it became a popular optical equipment for several applications, including dense wavelength division multiplexing (DWDM) [26], frequency measurement [27] and spectral slicing [7].

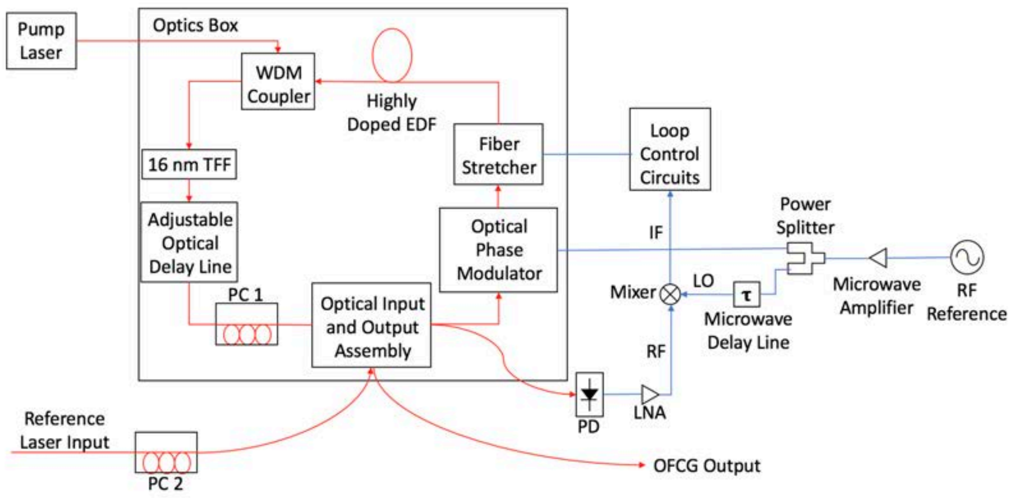

Fig. 1.6 Simplified block diagram of OFCG

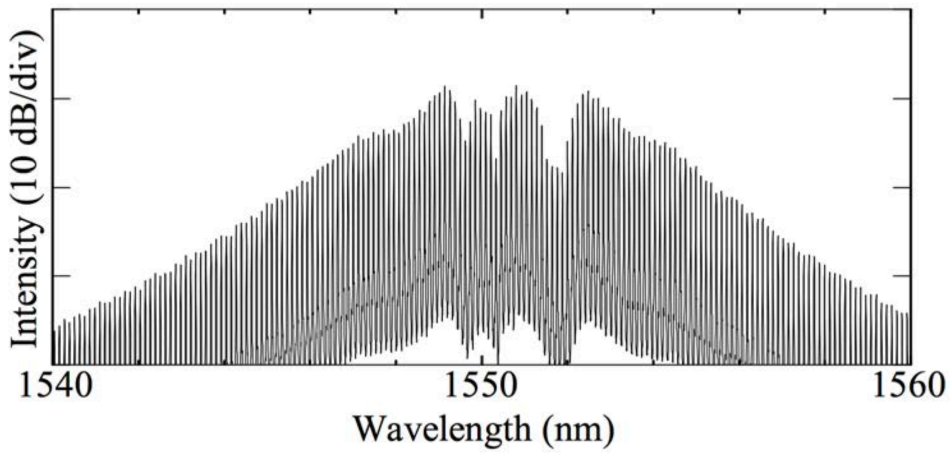

Fig. 1.7 Optical spectrum generated from OFCG in Morohashi's study [27]

Both frequency and phase locking characteristics of OFCG making it a popular component for different applications. Although recent research progress has improved flatness mismatch between comb-lines, making it able to handle stringent amplitude and phase matching requirement between sub-bands' spectrum, all comb-lines has to be generated by OFCG locally and eventually hindered the overall flexibility of architecture. Therefore, OFCG is widely adopted in WDM system rather than spectral slicing transmitter.

1.3.5 Spectral slicing receiver with independent lasers

Based on the drawbacks of OFCG, we are proposing a new architecture for spectral slicing transmitter, which may improve system's flexibility and performance as well. Proposed setup could be found in Figure 1.8.

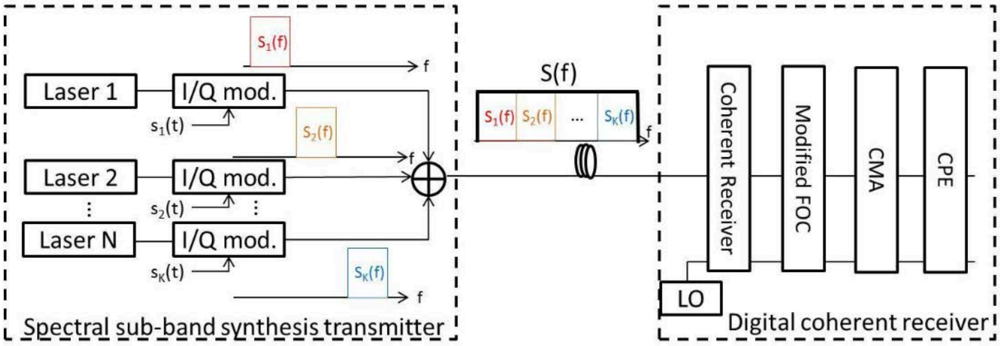

Fig. 1.8 Proposed setup of spectral slice transmitter

Comparing to Figure 1.7, OFCG was removed in our proposed setup. Instead of using single laser and other external hardware like de-multiplexer, frequency comb generator or frequency shifter, multiple lasers were used and modulated separately to form several sub-bands beforehand. Number of carrier used N in transmitter depends on number of sub-bands were used to reconstruct a large bandwidth signal S(f). For convenience in spectral slicing and frequency offset compensation, N was recommended to be 2^q, where q is any positive integer and such configuration will become conventional transmitter scheme when q = 0. Each laser was modulated separately with preprocessed slice of data from desired signal S(t), which were simply inverse Fourier transform of fraction of $S_i(f)$, where i = [1, N], forming sub-band spectra $S_1(f)$, $S_2(f)$, … $S_N(f)$. These spectra were then mixed at the output of transmitter, regenerating S(f).

Once S(f) was received at receiver, it will then be passed to our modified frequency offset compensation algorithm, along with constant modulus algorithm

(CMA) and carrier phase estimation (CPE) to retrieve clear constellation for decision.

1.4 Thesis outline

Given the complexity of the problem, this thesis will be divided into several chapters, each of them will address one issue at a time.

Chapter 2 introduced laser impairments. Origin of major impairments including laser phase noise (LPN) and frequency offset (FO), were discussed. Mathematical expressions of the impairments were also studied, showing impairments behavior and finding out major parameters contributing to signal distortions, thus stating the importance of digital signal processing.

Chapter 3 discussed the development of digital signal processing (DSP) and studied several classic widely adopted DSP algorithm for compensating FO and LPN. Their motivation, working principle, as well as corresponding algorithm performance, were studied via different perspectives.

With adequate understanding of major laser impairments and corresponding DSP algorithm for compensation, proposed configuration of spectral slicing transmitter was shown in chapter 4. Based on classic DSP algorithms and recent researches on frequency offset compensation, a DSP platform was proposed specially designed for spectral slicing transmitter composing of multiple independent lasers. Feasibility of the proposed configuration was first studied without influence of frequency offset, and performance of proposed DSP platform was studied with the proposed setup together later, with presence of independent FO in each transmitter lasers.

The final chapter concluded the entire thesis by summarizing discussions in chapter 2 & 3, achievement completed in chapter 4 and corresponding implication brought by the proposed configuration. A paragraph discussing possible future research directions was inserted in the final part.

Chapter 2

Laser Impairments in Fiber optic transmissions

2.1 Introduction

Increasing requirement for high bandwidth transmission has pushed the development of coherent communication components, especially opto-electronics components in transmitter as they were the major limiting factor, where signal degradation in transmitter has worse impact towards to signal quality than that in receiver. There are several linear impairments within transmitter and channel which could degrade the signal, such as frequency offset, laser phase noise and amplified spontaneous emission noise (ASE noise).

2.2 Simplified mathematical model of coherent communication systems

Figure 2.1 is a simplified block diagram showing some major impairments in coherent communication system which will be discussed in the following thesis.

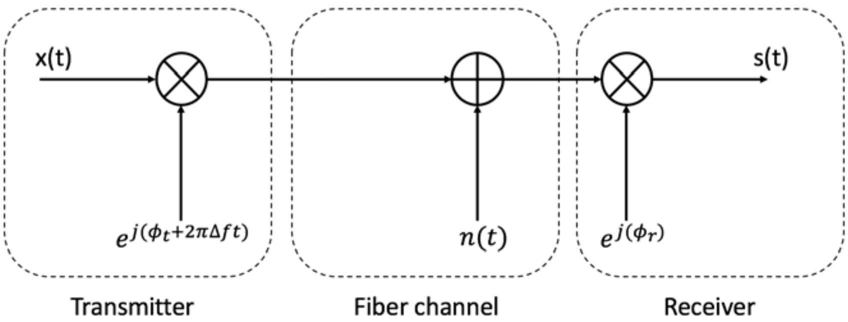

Fig. 2.1 Simplified block diagram of coherent communication system, where several impairments within fiber channel, such as chromatic dispersion (CD), polarization mode dispersion (PMD), were assumed completely compensated.

In above figure, laser phase noise ϕ_t and ϕ_r occurred in transmitter and receiver's local oscillator respectively. Along with ϕ_t, frequency offset Δf was also found in transmitter laser as well. Since laser beam was often amplified before being used in transmitter or receiver, ASE noise *n(t)* was included in our model as well. At transmitter output, transmitted signal $x_t(t)$ could be written as:

$$\boldsymbol{x_t(t) = x(t)\ e^{j(\phi_t + 2\pi\Delta f t)}} \qquad (2.1)$$

Considering that ASE noise behaving similarly to Additive White Gaussian Noise (AWGN), it can be extracted from the equation and simplified as a separate term. With the presence of laser phase noise in receiver end, received signal *s(t)* could be written as below:

$$\boldsymbol{s(t) = x(t)\ e^{j(\phi_t + 2\pi\Delta f t)}\ e^{j(\phi_r)} + n(t)} \qquad (2.2)$$

which could be further derived into:

$$\boldsymbol{s(t) = x(t)\ e^{j(\phi_t + 2\pi\Delta f t + \phi_r)} + n(t)} \qquad (2.3)$$

where all terms in above expressions are in time domain, *x(t)* and *s(t)* are both complex signals, depending on modulation format; Laser phase noise in both transmitter and receiver, ϕ_t and ϕ_r, are in units of radian (rad) and frequency offset Δf is in unit of Hertz (Hz).

2.3 Laser phase noise (LPN)

Phase noise is one of the critical linear impairment within coherent communication system as it leaded to carrier synchronizing issues. Back in the days where IM-DD is popular, laser phase noise (LPN) was not attractive as only light intensity was detected and measured in receivers. However, for modulation format applied in coherent communications, especially QAM and PSK signals, phase is used for encoding data. Thus, LPN may cause transmission error and introducing the requirement of low linewidth laser for communication usage.

The origin of LPN was quantum noise, especially spontaneous emission in lasers' resonators, same origin as ASE noise [28]. Evolution of LPN could be viewed as Wiener process [29]. Consider a laser suffering from LPN only, where transmitted signal $x_{t,PN}(t)$ will be distorted from original signal x(t):

$$\boldsymbol{x_{t,PN}(t) = x(t)e^{j\,\phi(t)}} \tag{2. 4}$$

where $\phi(t)$ is instantaneous phase noise of laser, $x(t)$ and $x_{t,PN}(t)$ are complex signals. $\phi(t)$ development could be regarded as Wiener process and could be written as follow:

$$\boldsymbol{\phi(t) = \int_{-\infty}^{t} \delta\omega(\tau)d\tau} \tag{2. 5}$$

where $\delta\omega(t)$ denotes frequency noise, with zero mean and variance of $2\pi\Delta\nu dt$. $\Delta\nu$ and dt indicating 3 dB laser linewidth of Lorentzian-shape spectrum laser (in Hz) and symbol period (or reciprocal of baud rate) respectively.

Through investigating the expression in equation 2.5, it can be summarized that instantaneous phase noise of laser is accumulated sum of frequency noise increment. Together with the property of Wiener process, where $\delta\omega(0)$ is set to zero as initial point. Summarizing above conditions of Wiener process helped us to model LPN, where several examples were included in Figure 2.2.

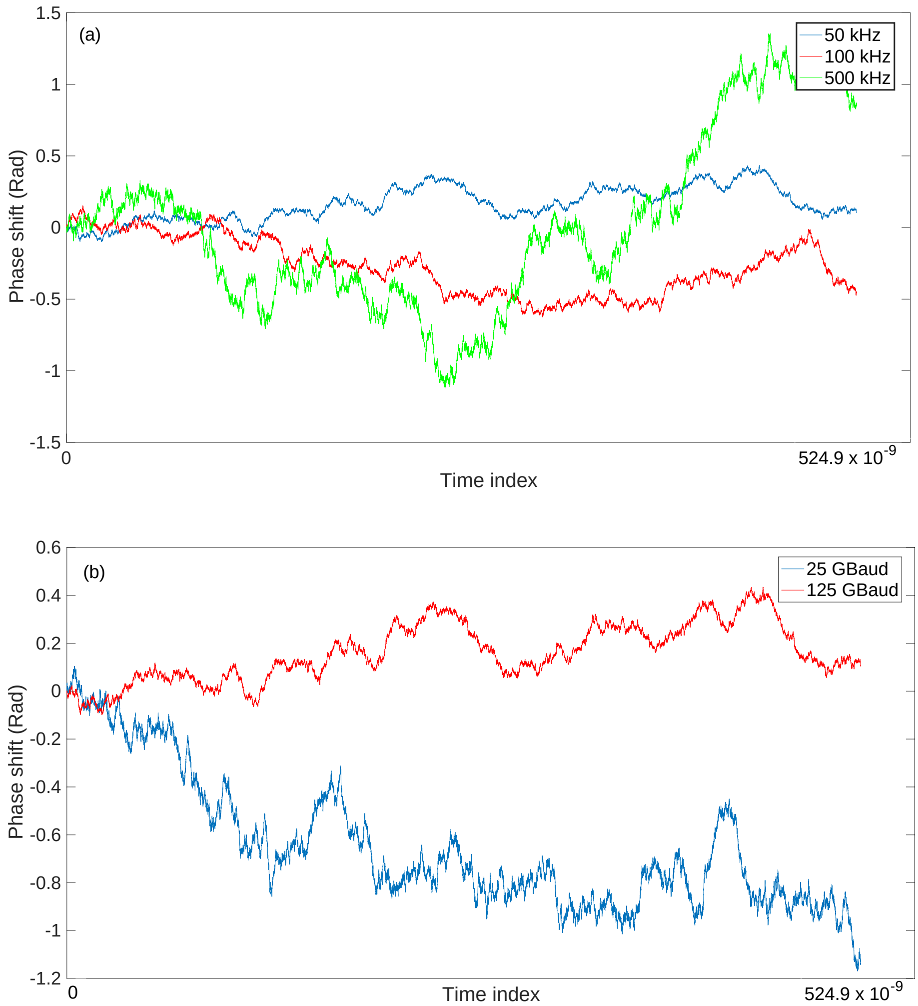

Fig. 2.2: Relation between evolution of LPN and respective parameters: (a) Laser linewidth; (b) Baud rate. Baud rate was set at 125 GBaud in (a) and laser linewidth was set to 50kHz in (b).

Equation 2.5 stated the instantaneous phase noise, or LPN for certain time index, was based on phase shift of the previous time index. Increment from previous time index was Gaussian distributed with zero mean and variance proportional to laser linewidth and symbol period. From figure 2.2 (a), larger increment of phase shift could be observed when laser linewidth increased from 50 to 500kHz. Meanwhile, same phenomenon could be observed in figure 2.2 (b), when symbol rate was reduced, increasing symbol period, would leaded to larger variance in distribution as well as larger increment, thus drifting away from initial zero position.

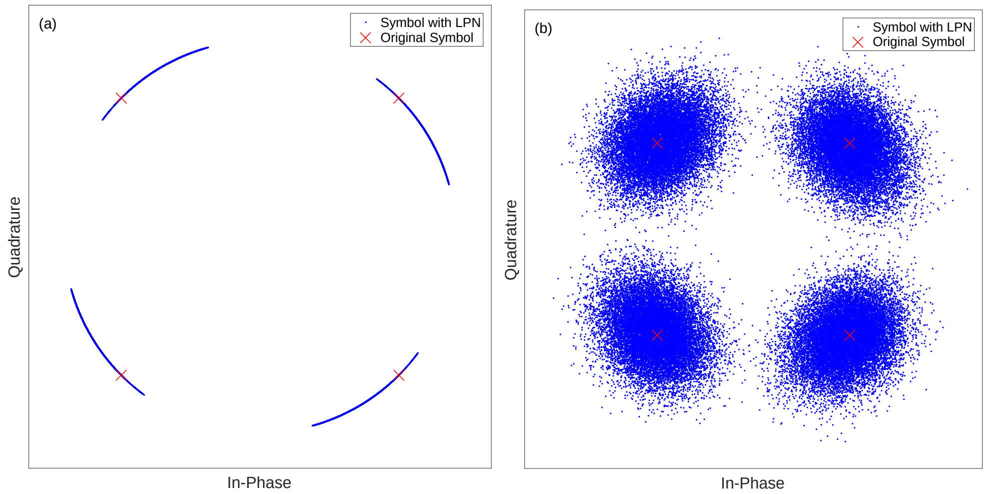

Fig. 2.3 Constellation plot of QPSK signal, comparing original position and corresponding distribution after suffering from transmitter LPN: (a) Without ASE noise; (b) With ASE noise. Linewidth, baud rate and OSNR were set to 100 kHz, 125 GBaud and 22 dB respectively. Receiver LPN and frequency offset were absent.

Figure 2.3 showing impact brought to symbol distribution brought by transmitter LPN. As stated in equation 2.4, LPN could be treated as a simple rotation and keeping same radius, if was considered independently. The degree of rotation is totally random and can be considered as an accumulated sum with starting at zero. The size of its increment is Gaussian distributed, with zero mean and variance depends on laser linewidth and symbol period. Although rotation in this figure is mild and no any distorted symbols fell to neighbor decision region, this may happen if other parameters were considered, such as receiver LPN and frequency offset, resulting in decision error and eventually bit error.

2.4 Frequency offset (FO)

Compared to Laser phase noise (LPN), discussed in session 2.3, which causing continuous random phase rotation in time domain or continuous frequency shift in frequency domain, frequency offset (FO) comes with different origin and different properties as well.

Generally, FO arise from several factors, such as operating temperature, frequency locking in lasers, frequency mismatch between transmitter and receiver lasers, or even Doppler effect for moving transmitter or receiver.

For given original complex signal *x(t)*, transmitted signal $x_{t,FO}(t)$ will be distorted as follows:

$$\boldsymbol{x_{t,FO}(t) = x(t)\ e^{j(2\pi\Delta f t)}} \tag{2. 6}$$

where Δf denotes the frequency offset from designated carrier frequency (in units of Hz) and t denotes time elapsed for the complex symbol transmission.

Comparing equation 2.4 and 2.6, similar behavior of LPN and FO can be concluded, where original symbols experienced a constant modulus rotation. However, rotation induced by LPN was a Wiener process, where instantaneous phase noise of certain symbol depends on instantaneous phase noise of the previous symbol and corresponding increment was decided by laser linewidth and symbol period. Instead of a continuous, random process, FO is a rotation which entirely depends on the frequency mismatch. Considering the phase shift term within the bracket in equation 2.6 and differentiate with respect to time, evolution of phase shift due to FO could be realized, which is linear with a slope of $2\pi\Delta f$.

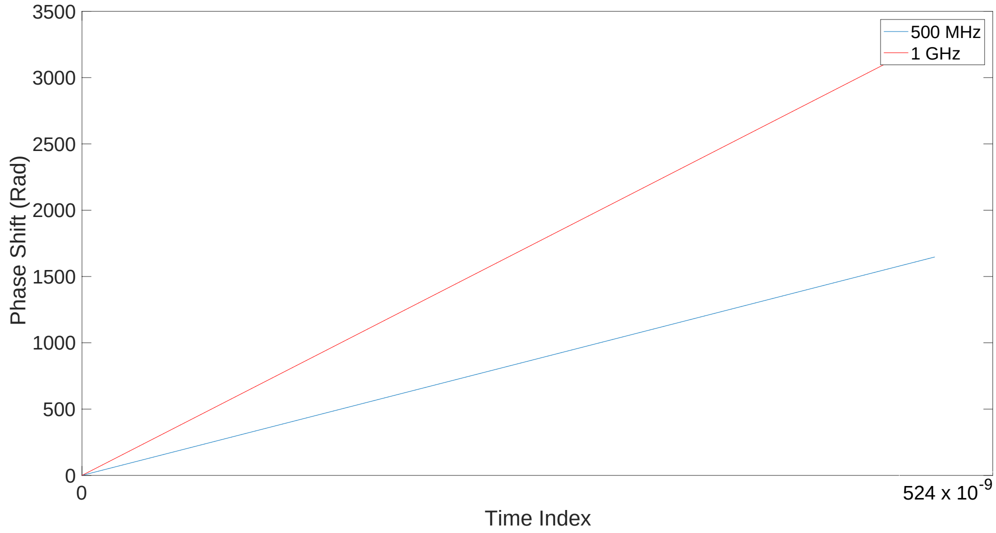

Fig. 2.4 Development of phase shift due to different frequency offset (FO): (a) 500 MHz; (b) 1 GHz

Comparison on phase shift development based on different frequency offset was shown in figure 2.4. As stated above, it developed linearly instead of randomly with Gaussian distributed increment. Besides, comparing y-axis value in figure 2.4 to that of 2.2, FO brought greater impact on symbol distortion than LPN. With a several thousands of radians rotation on symbols, it is difficult for receiver to perform direct decision on received symbols without any frequency offset compensation. Constellation plot showing symbols suffering from FO was shown in figure 2.5.

Although evolution of FO induced phase shift is linear, it is difficult to completely compensate FO with presence of other distortion sources, such as LPN and ASE noise. Figure 2.6 showed the difference of phase shift evolution from one and multiple distortion source. Above figure suggested that retrieval of FO simply by calculating phase shift in pilot symbol with LMS fitting may induce great error, which eventually lead to detection error.

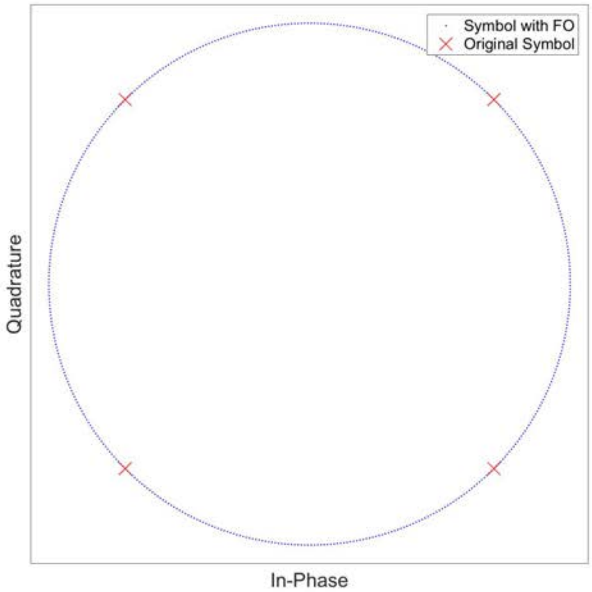

Fig. 2.5 Constellation plot of QPSK signal, comparing original position and corresponding distribution after suffering from FO. FO was set to 500 MHz. Transmitter and receiver LPN, ASE noise were absent.

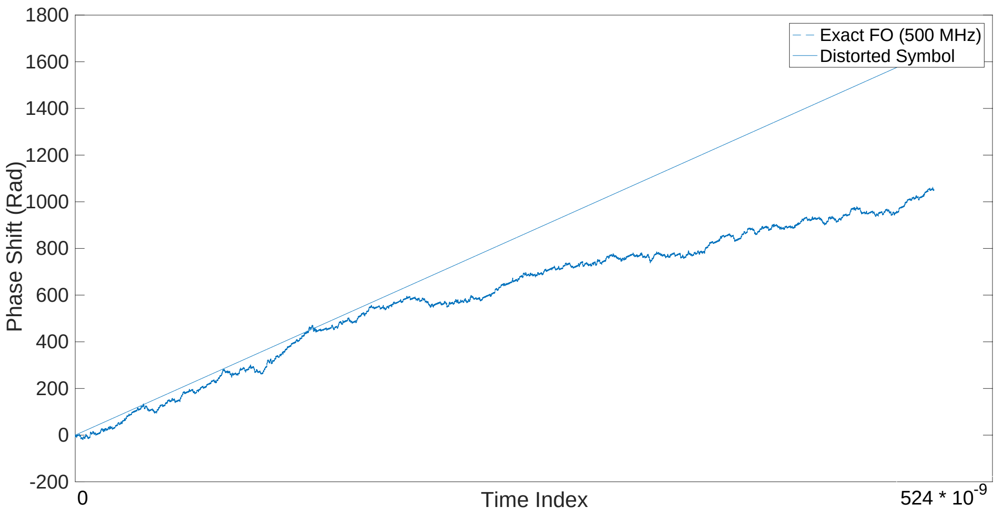

Fig. 2.6 Comparison of FO development: (a) With FO only; (b) Sum of several signal distortion source, including transmitter and receiver LPN, FO and ASE noise. ASE noise was set to 22 dB; laser linewidth was set to 100 kHz and baud rate was set to 125 GBaud.

Chapter 3

Digital Signal Processing Algorithm for Linear Impairment

3.1 Introduction

Previous chapter explained various distortion investigated throughout the entire thesis. Though most of those distortions are uniform rotation, it will be difficult to compensate to acceptable level if all of them were considered, including transmitter and receiver LPN, FO, and ASE noise, where comparison of phase shift development between multi source distortion and single source distortion were shown in figure 2.6.

Besides, as discussed in previous chapter, adopting advance modulation format may ease the demand on DAC bandwidth. Though we have lasers in the laboratory possessing linewidth of around 10 kHz and 1 kHz [30] [31], most commercially available continuous wave (CW) laser having a linewidth of 50 – 100 kHz linewidth for external cavity lasers (ECL). Higher order modulation format usually requires more robust and adaptive DSP algorithm due to smaller error margin. Figure 3.1 showed constellation plot of QPSK and 16QAM. Though 16-QAM can provide double bit rate under same symbol rate, QPSK symbols has higher phase noise tolerance of $\frac{\pi}{2}$, while middle ring of 16-QAM symbols can only withstand $\frac{\pi}{4}$ rotation, showing the importance of DSP algorithm development.

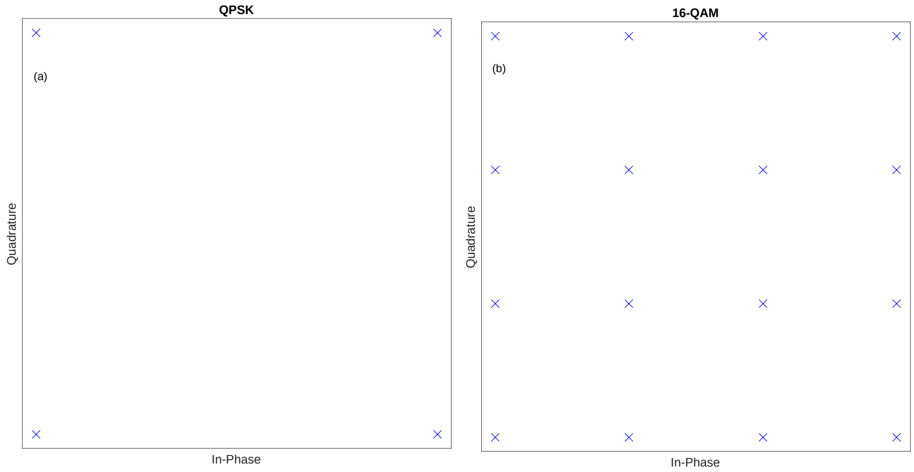

Fig. 3.1 Constellation plot of different modulation format: (a) QPSK; (b) 16QAM

3.2 Constant modulus algorithm (CMA)

Being one of the blind adaptive equalization approaches, CMA does not require any training or pilot symbols, making it popular for linear time invariant (LTI) channels. Besides LPN and FO, distortions caused by lasers, inter symbol interference (ISI) is also an important distortion in coherent communication systems. ISI is a phenomenon where a symbol was distorted by one another, mainly due to limited bandwidth of channel, or imperfect fiber which eventually causing polarization mode dispersion (PMD). To tackle channel distortions, CMA is often used, through numerical approaches, to linearly approximate and mimic a filter which similar to inverse of channel's transfer function. Moreover, the adaptive characteristics of CMA allowed it to track changes in transfer function, which varies slowly. CMA was first investigated by Godard in the 80s [32] for equalization of QPSK signal in the beginning and application on polarization multiplexed (Pol-Mux) signal was left open. Subsequently, it was applied to Pol-Mux signal with a 4 by 4 matrix which act as a MIMO equalizer.

Under the family of adaptive equalizers, there are other algorithms beside CMA as well, such as least mean square (LMS), recursive least squares (RLS). Although their structures were simpler, training symbols are required for both LMS and RLS, which reduced system throughput eventually. Hence, absence of training is preferred for adaptive equalization and received signal properties is often taken for channel estimation and saved overhead.

Figure 3.2 showed a MIMO equalizer for Pol-Mux signal equalization. Consider a Pol-Mux signal where x and y polarization containing independent signal. This MIMO equalizer is mainly used for equalizing channel distortion h, including PMD, which can be regarded as rotation of polarization axis. Hence to retrieve x and y polarization's signal, a 2 input, 2 output MIMO equalizer with 4 filter tap weights (h_{xx}, h_{xy}, h_{yx} and h_{yy}) is adopted and corresponding outputs are:

$$\begin{cases} \boldsymbol{x_{out}[k] = h_{xx}^{H} x_{in}[k] + h_{xy}^{H} y_{in}[k]} \\ \boldsymbol{y_{out}[k] = h_{yx}^{H} x_{in}[k] + h_{yy}^{H} y_{in}[k]} \end{cases} \qquad \boldsymbol{(3.1)}$$

where each filter tap weight is 1xN matrix and equalizing x and y polarization input signal in a block by block manner that N symbols from both polarization was taken, hence $\boldsymbol{x}_{in}[k] = [x_{in}[k], x_{in}[k-1], x_{in}[k-2], \dots, x_{in}[k-N]]$.

Consider a 2 by 2 matrix H containing the four filter tap weights, which tried to approximate the rotational condition:

$$\boldsymbol{H} = \begin{bmatrix} \boldsymbol{\cos\theta} & \mathrm{e}^{-\mathrm{j}\phi}\boldsymbol{\sin\theta} \\ \mathrm{e}^{-\mathrm{j}\phi}\boldsymbol{\sin\theta} & \boldsymbol{\cos\theta} \end{bmatrix} \qquad \boldsymbol{(3.2)}$$

where 2θ and ϕ denoted horizontal and elevation angle of rotation respectively. Both equal to zero in ideal condition. Thus, the k^th^ element in initial tap weight of h_{xx} and h_{yy} were set to 1, while h_{xy} and h_{yx} were set to 0.

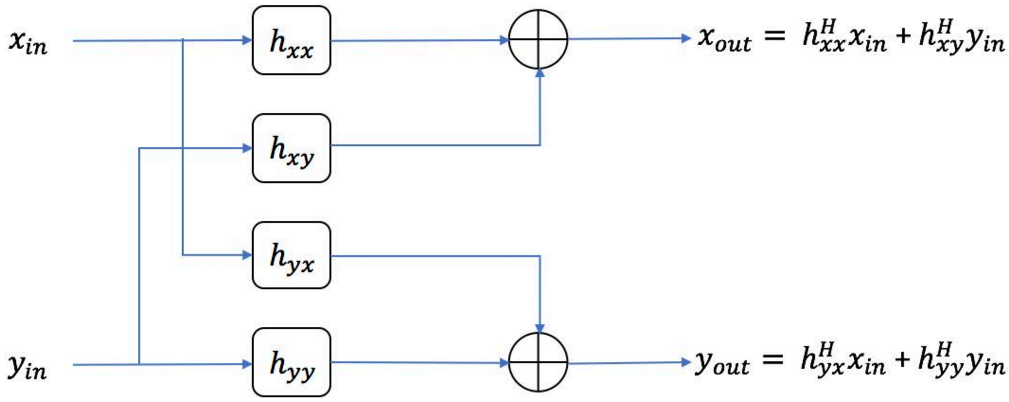

Fig. 3.2 MIMO equalizer

As CMA's objective is to blind equalize signal based on constant modulus criterion, which was often set to 1 for simplicity, cost function can be generated as follow:

$$\begin{cases} \varepsilon_x^2 = (1 - |x_{out}^2|)^2 \\ \varepsilon_y^2 = (1 - |y_{out}^2|)^2 \end{cases} \tag{3.3}$$

Although various update algorithm was proposed in the past [33], stochastic gradient descent method was the majority as it provides global convergence. For simplicity, we only investigated stochastic gradient descent update algorithm in this section. By selecting proper step size μ, filter taps could be updated as follows:

$$\begin{cases} \boldsymbol{h_{xx}} := \boldsymbol{h_{xx}} - 2\mu\varepsilon_x\overline{\boldsymbol{x_{in}}}\boldsymbol{x_{out}} \\ \boldsymbol{h_{xy}} := \boldsymbol{h_{xy}} - 2\mu\varepsilon_x\overline{\boldsymbol{y_{in}}}\boldsymbol{x_{out}} \\ \boldsymbol{h_{yx}} := \boldsymbol{h_{yx}} - 2\mu\varepsilon_y\overline{\boldsymbol{x_{in}}}\boldsymbol{y_{out}} \\ \boldsymbol{h_{yy}} := \boldsymbol{h_{yy}} - 2\mu\varepsilon_y\overline{\boldsymbol{y_{in}}}\boldsymbol{y_{out}} \end{cases} \tag{3.4}$$

With above signal modelling and filter tap update equation, symbols could be equalized to constant modulus. Figure 3.3 showed CMA result of QPSK and 16QAM, showing CMA's convergence and format independent ability. Global convergence property of CMA made itself aa popular blind adaptive equalizer for channel estimation and high performance is guaranteed. However, CMA employed constant modulus criterion that equalize symbols through adjusting power ratio of two polarizations, and $\frac{\pi}{2}$ ambiguity in equalized symbols were shown by Savory [34]. Such ambiguity will rotate a series of symbols, behaves similar to cycle slip and difficult to be detected.

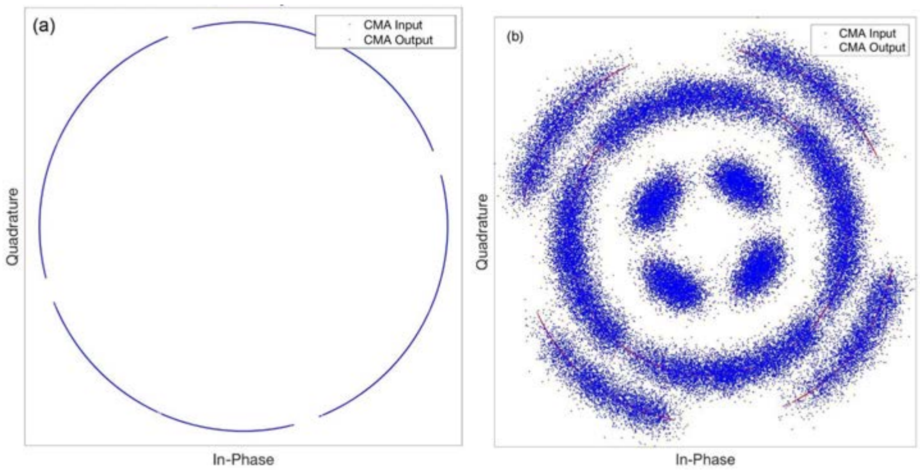

Fig. 3.3 CMA input and output of (a) QPSK signals and (b) 16QAM signals. Laser linewidth was set to 100kHz and ASE noise was absent.

3.3 Frequency offset estimation algorithm (FOE)

Recent advance in laser technologies reduced noise from various origins. Consider an external cavity laser (ECL) for telecommunication applications, its frequency resolution is as small as about 375MHz with proper frequency locking and temperature stabilization [35], which is a considerable improvement where 1 GHz offset was often set for simulation in the past. Although frequency offset was reduced compared to past, it is still greater than the tolerance stated by most of the CPE algorithms, thus accurate phase estimation could not be performed under such conditions. Hence, proper FOE is required before CPE to compensate carrier frequency offset to reduce residual FO within CPEs' tolerance range.

Like CPE, modulation format need to be removed for most FOE algorithms, before frequency offset estimation, which can be classified as data aided or non-data aided approach. Generally, non-data aided approach is more popular as no overhead is needed, preserving spectral efficiency. One of the classic approaches is to search for the spike in the spectrum of M^{th} power processed signal, which indicates the maximum power, and calculate offset from original position [36]. Processed signal can be expressed as follows:

$$\boldsymbol{z_k} = (\boldsymbol{x_k})^{\boldsymbol{M}} = \boldsymbol{e}^{\boldsymbol{j}(\boldsymbol{2M\pi\Delta fkT+\phi})} + \mathbf{n}(\mathbf{k}) \qquad (\mathbf{3.5})$$

where x_k denotes received signal from receiver, Δf is frequency offset, T indicating symbol period, ϕ and n are LPN and AWGN respectively. Considering a QPSK signal was received, x was raised to the power of four, removing modulation and leaving series of error vector z. Maximum likelihood (ML) estimator with feedback delay L can then be implemented to approximate FO Δf through finding maximum position of overall spectrum and compare to original position (carrier frequency). Calculation of FO is expressed below:

$$\widehat{\Delta \boldsymbol{f}_{\boldsymbol{k}}} = \boldsymbol{argmax}\left\{\left|\frac{\mathbf{1}}{\boldsymbol{L}}\sum_{\boldsymbol{n=0}}^{\boldsymbol{L-1}} \boldsymbol{z_n}\boldsymbol{e}^{\boldsymbol{j2\pi\frac{nk}{N}}}\right|\right\}, \mathbf{k} = \mathbf{1}, \mathbf{2}, \ldots, \mathbf{L-1} \qquad (3.6)$$

3.3.1 Non-data aided FOE

With years of development in FOE algorithms, they could be classified into Non-Data and data aided FOE today. Acting as base of signal demodulation, NDA FOE having an advantage of no pilot symbols or any information are needed, hence suitable for different applications, like satellite communications.

Maximum likelihood (ML) estimator was often used in NDA FOE algorithms [37] [38] [39]. Although NDA ML estimator having higher Cramer-

Rao Lower Bound (CRLB) than DA ML estimators, NDA ML estimator is proved able to attain corresponding lower bound due to absence of pilot symbols, making the estimator unbiased and achieving the lower bound only if sufficient length of symbols was included or sufficient SNR [40].

Besides implementation of ML estimator, others approaches were adopted to achieve non-data aided estimation, including offset estimation exploiting received symbols' instantaneous phase noise and corresponding probability density function [41]. Another method, proposed by Leven [42] and corresponding block diagram shown in figure 3.4, eliminated modulation format by powering received symbols to M-power and retrieving corresponding argument, which is similar to equation 1.18. The major difference is calculation of FO is based on differential summation where multiplication of complex conjugate was included. Such method brought great influence to development of FOE algorithms, where variants were proposed, including dual stage FOE of modified Leven approach [43].

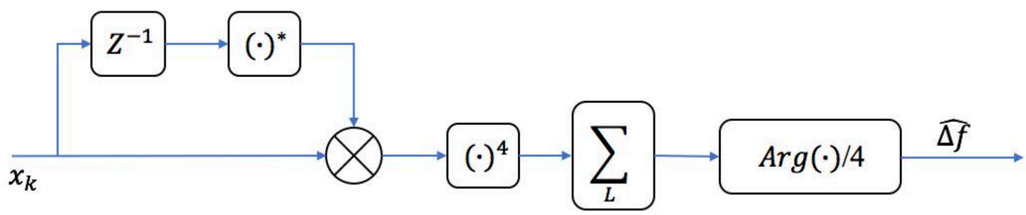

Fig. 3.4 Block diagram of FOE algorithm proposed by Leven [42]

Through raising the entire signal to the power of four and finding average value of phase difference of the current received and the previous symbol, modulation was removed and FO was estimated. However, principle behind this algorithm implied it could not be applied to higher order format, like 16-QAM or

32-QAM, as it based on symbols' $\frac{\pi}{4}$ offset from the axis. Improvement on such algorithm was needed to overcome the more stringent requirement on FO tracking ability with higher order modulation format.

To tackle drawbacks of Leven's approach [42], two stages FOE algorithm was proposed. Figure 3.5 showed the schematics of the proposed FOE method [43]. The first stage provided a rough estimate of FO by calculating phase discrepancy among received symbol and the previous symbol, where the entire signal was roughly compensated according to the approximate value. Second stage was then implemented with similar approach, while average value was calculated using received symbol and another symbol with delay L, hence providing an accurate estimate of FO. Both stages were developed based on symbols' phase discrepancy, where the first stage calculate with two consecutive symbols, and the second stage employed symbols with L symbol distance between after coarse compensation in the first stage. Implementation of the second stage provided accurate FO estimation, as well as noise tolerance originating from imperfect compensation of other signal distortions and AWGN. With these advantages, such approach was proven to be able to be applied on 16-QAM as well, by treating the middle ring symbols as QPSK signals with extra LPN.

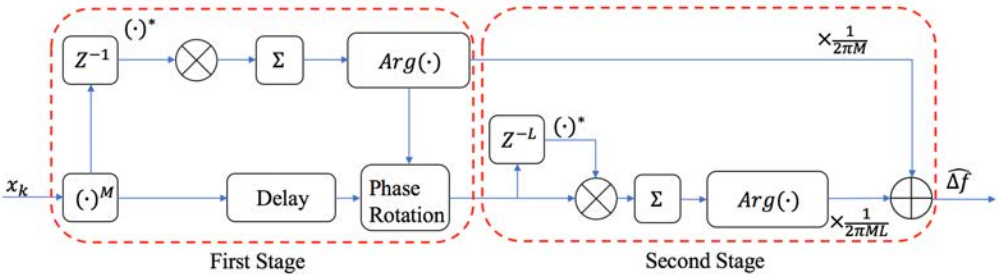

Fig. 3.5 Block diagram of two stage FOC algorithm proposed in [43]

3.3.2 Data aided FOE

Although Non-data aided FOE save spectral efficiency and can be applied in different application where pilot symbols are not available. However, NDA FOE shared a common problem where their tolerance of estimation range limited by constellation stages and symbol period [44]. Hence, data-aided FOE was not completely replaced yet as it can provide even higher accuracy and enables channel estimation through exploiting pilot symbols or pilot tones. For single carrier coherent optical communication systems, method was proposed to compensate CFO with the presence of pilot tone [45]. Drawback of such method is extra laser is needed for pilot tone, which eventually hindered flexibility of system.

As such, improved FOE was proposed to tackle problem brought by employing an extra pilot tone [46]. Figure 3.6 showed data frame structure to create pilot tone. Consider certain frame within the entire transmitted signal, where a string of pilot symbols, for FOE, were inserted before transmission of payload, containing information to be transmitted. Through choosing a non-zero symbol of designated modulation format arbitrarily and repeat it for several times, depends on length of pilot symbols inserted, will generate a pilot tone-like spike on transmitted spectrum which was then retrieved for FOE.

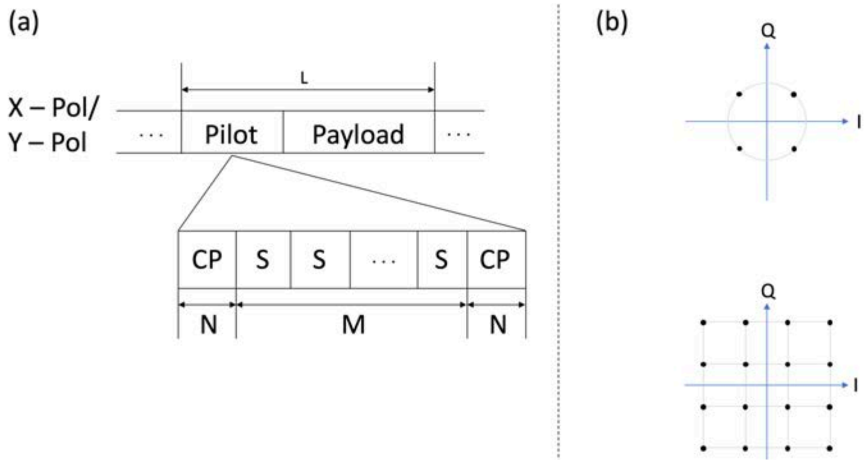

Fig. 3.6 DA FOE based on pilot tone approach [46] (a) Data frame structure; (b) Constellation plots of popular modulation format

Based on the band selecting characteristics of channel, pilot symbols were inserted intentionally in a periodic manner, such that harmonics of pilot tone was filtered and only DC component of pilot tone was remained for FO calculation. Transmitted payload and pilot tone were depicted in figure 3.7, showing effect of CFO to the overall transmitted spectrum.

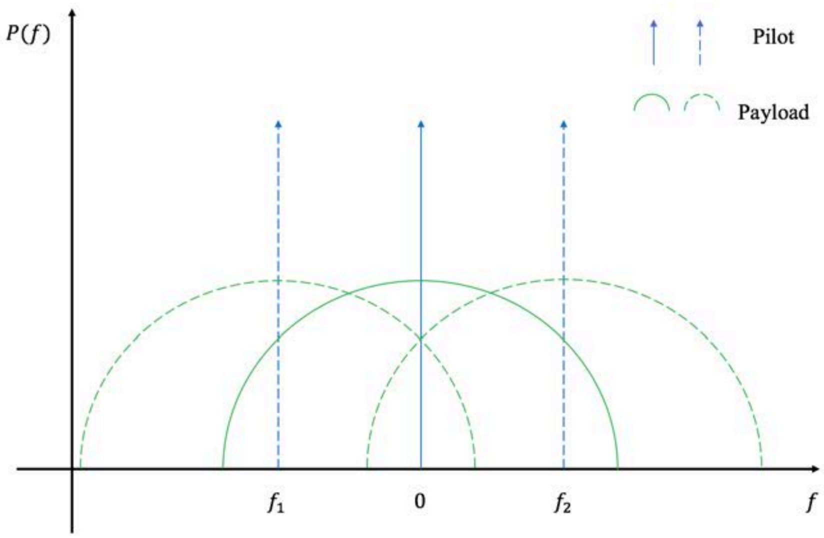

Fig. 3.7 Effect of Frequency offset done to transmitted spectrum. Solid line represented ideal transmission, while dashed lines represented transmitter spectrum experienced FO of Δf, either left or right.

3.4 Carrier phase estimation algorithm (CPE)

Given that LPN was one of the major linear impairment causing bit error in coherent communication systems, carrier phase estimation algorithm, or CPE, was considered as a key component in DSP algorithm family in coherent communication systems for combating LPN in both transmitter and receiver.

Consider a radio communication system, where usually a phase lock loop (PLL) together with a single tap least mean square (LMS) filter were implemented to achieve phase synchronization. Modulation format was removed from received symbol, thus corresponding phase rotation can be estimated. Various approaches could be adopted to perform phase estimation in PLL, including raising power of received signal to M-th power for M-PSK signals [47]. With control signal from the feedback loop, decision directed phase estimation was employed to perform phase synchronization in radio communication system. Based on the similarity between optical coherent communication system and radio communication system, same principle could be applied in optical coherent communication system as well. Figure 3.8 showed a block diagram of single tap LMS filter for phase synchronization. Received symbol r(k) with certain phase angle $\phi(k)$ was received and undergo decision as decided symbol $r_{dec}(k)$ with predefined angle $\phi_{dec}(k)$. Phase difference between $\phi(k)$ and $\phi_{dec}(k)$ was treated as phase noise for symbol r(k) and was feedback to correct later receiver symbols r(k+N), where N was defined as feedback delay and depended on the hardware structure of feedback loop and algorithm architecture.

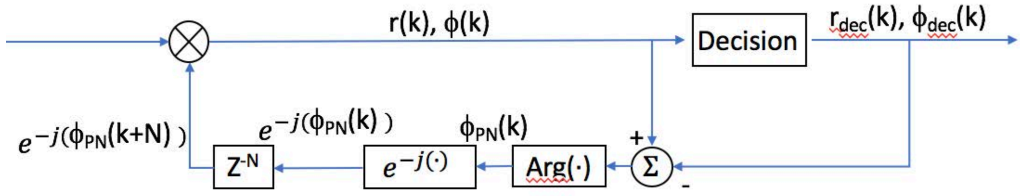

Fig. 3.8 Block diagram of single tap LMS filter for phase synchronization

However, given that most of the integrated chip can only provide a fraction of required processing speed, parallelization is often required, which ended up in increasing system complexity as well as feedback delay. Besides, LPN-induced distortion may be occurred in the feedback loop due to hardware and algorithm architecture. Hence, CPE algorithms like Viterbi-Viterbi phase estimation was commonly used in receiver end to reduce number of ASIC, to reduce hardware or software complexity and eventually reducing feedback delay in receiver.

3.4.1 Viterbi-Viterbi phase estimation (VVPE)

Among various CPE algorithm, Viterbi-Viterbi phase estimation is regarded as one of the popular algorithm [48]. Considering a train of symbols with other impairments compensated, including chromatic dispersion (CD), polarization mode dispersion (PMD), FO, and was down-sampled to original baud rate. Assuming the k^{th} symbol r(k) was transmitted along certain polarization and was fed to CPE algorithm, could be expressed as follows:

$$\boldsymbol{r(k) = x(k)e^{j(\phi(k))} + n(k)} \qquad \boldsymbol{(3.7)}$$

where x(k) was the k-th complex symbol transmitted from transmitter, n(k) indicating ASE noise which behaves as a two-dimensional random vector; $\phi(k)$ is a sum of LPN, which originates from both transmitter and receiver LPN, $\phi_t(k)$ and $\phi_r(k)$ separately.

Considering a Quadrature Phase Shift keying (QPSK) Signal, the k^{th} signal x(k) was written as follow:

$$\boldsymbol{x(k) = Ae^{j(\theta(k)+\phi(k))}} \qquad (3.8)$$

where A is the amplitude, or modulus, of the QPSK symbol, which usually is $\sqrt{2}$ or can be normalized to 1, while $\theta(k)$ denotes the argument of QPSK signal and equal to $\pm\pi/4$ or $\pm 3\pi/4$, based on the format definition.

Given the fact that these phase offsets are factors of π and $\frac{\pi}{2}$, received symbol's format could be removed, by applying De Moivre's Theorem and raising x(k) to the power of 4. Thus, the following expression could be found:

$$\boldsymbol{\mathrm{r}^4(k) = e^{j\left(4\theta(k)+4\phi(k)\right)} = e^{j\left(4\phi(k)\right)}} \qquad (3.9)$$

At this point, modulation has been removed and ideal demodulated symbols will lie on the In-Phase axis. If any impairments in symbols causing rotation, angle will be formed between unmodulated received symbols and In-Phase axis, as shown in Figure 3.9. Once the angle is formed, phase noise of the k^{th} symbol could be retrieved and used for carrier phase compensation, by dividing 4, the power raised on symbols in earlier stage. Figure 3.10 showed a detailed block diagram showing the flow of VVPE.

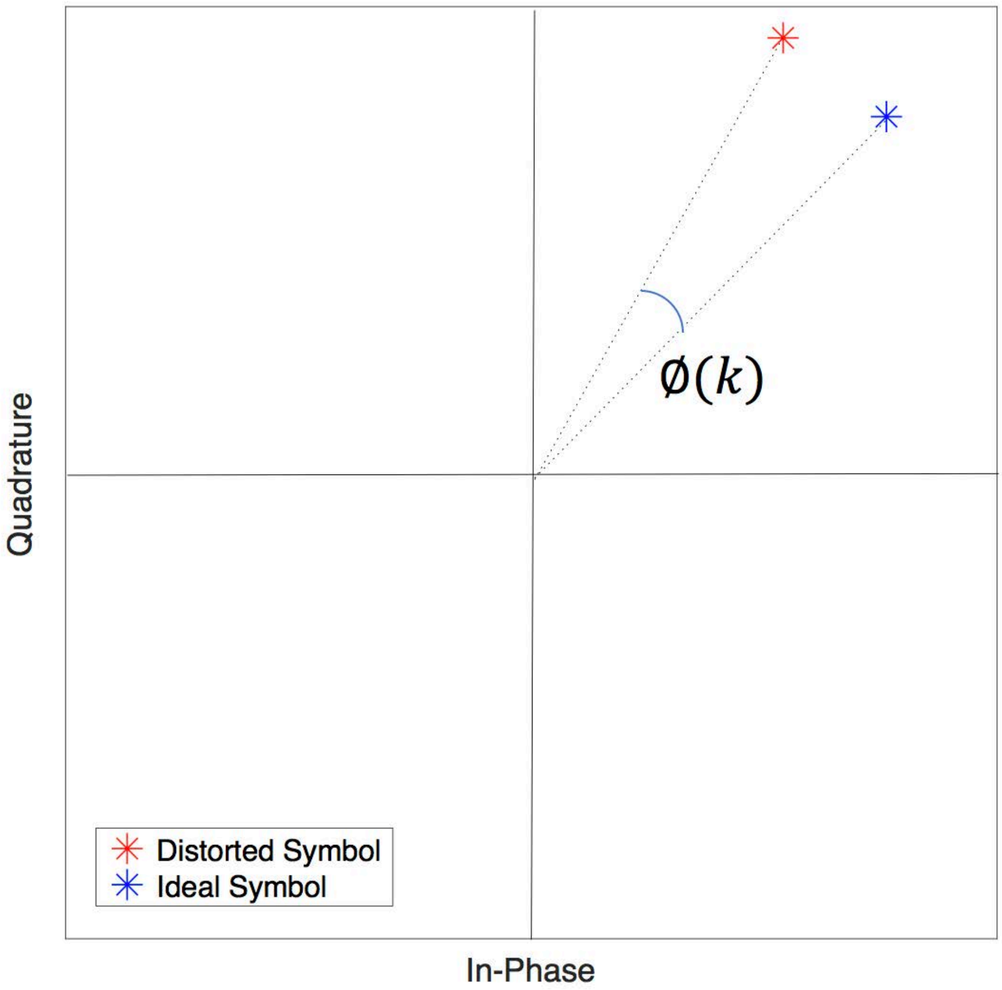

Fig. 3.9 Output of VVPE, indicating angle between symbols and in-phase axis, in case of any distortion occurs

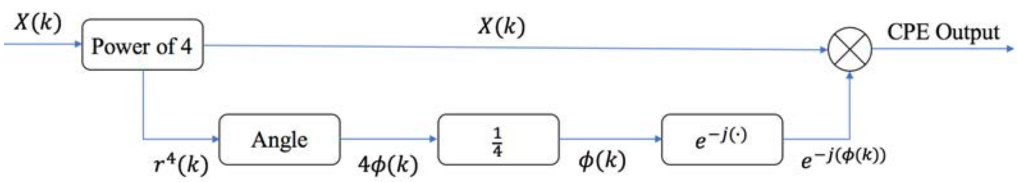

Fig. 3.10 Block diagram of VVPE

Though VVPE eased the complexity in receiver structure as well as feedback delay, VVPE is only limited for synchronizing QPSK signal as it exploited the argument and position of symbols. If advance formats were adopted like 16 or 64-QAM, VVPE cannot estimate phase noise of symbols precisely. To handle this drawback, researchers made several modifications on VVPE to allow it to be applied on higher order square QAM format as well, such as VVPE with (enhanced) maximum likelihood estimator (VVPE-ML) for 16-QAM and 64-QAM symbols, together with QPSK-Partitioning Approach [49], [50], and VVPE with Extended Kalman filter (VVPE-EKL) for 16-QAM symbols [51].

3.4.2 Blind phase searching algorithm (BPS)

Besides VVPE, different variants of VVPE, other feedforward or feedback and other CPE algorithms [52] were researched extensively to synchronize carrier with different modulation formats, such as QPSK [48], [53], 16-QAM [54] [55] [56] [57] [58] [59], and higher order QAM signals [59] [60] [61]. As mentioned in the introduction section, exponential increase of internet traffic in the following decade is predicted and higher flexibility is expected, extensive researched has been conducted on elastic optical networking and software defined networking [62] [63] [64].

Thus, a format independent DSP platform is expected and desired for next generation software defined networking, which researchers had to develop novel approaches and ideas to facilitate this demand. There are format independent DSP algorithms for several distortions, including blind estimation of chromatic dispersion (CD) [65] [66], FFT-based frequency offset estimation [67] and CMA, while format independent CPE like BPS was not proposed until 2014 [68], which could be applied to a general M-QAM format instead of limited to particular QAM format, like QPSK partitioning for 16 or 64-QAM signal [49] [50], or VVPE with Extended Kalman filter for 16-QAM signal only [51].

Generally, a DSP platform could be divided into two parts. The first part included a rapid, format independent impairment compensation, while the second part composed of a tracking mechanism which enables the tracking of gently evolving distortions. BPS belongs to the early one as it also helped format identification after pre-convergence, hence respective DSP algorithm could be selected to compensate the slow varying distortions. Comparing other distortions, LPN possessed relatively larger variation over certain amount of time, indicating the needs for format independent CPE [69].

BPS adopted the concept of parallelization, which was shown in figure 3.11. In practical application, available equipment could not process received data in high speed to achieve low feedback delay. Through arranging a set of low speed parallel modules in receiver, received data could be de-multiplexed, forwarded and handled by modules, thus reducing feedback delay.

Figure 3.12 showed a block diagram of BPS. Consider a set of test carrier phase was set, as an analogy to parallel modules in receiver, received symbol was duplicated and rotated by different angle of the test carrier phase set. These rotated symbols were then passed to a decision circuit and distance between each rotated symbol and corresponding closest constellation point was calculated. To reduce performance degradation due to other sources of distortion, estimated distance of consecutive symbols were added improve BPS’s noise tolerance. By comparing the summed distance values within the set, optimum laser phase noise could be approximated by picking the minimum value. Given that decision circuit was used in early stage of the algorithm, compensated symbols could be picked from the decision output of the optimum test carrier phase value.

Due to the feedforward characteristics of BPS, feedback loop was avoided and result in relatively higher phase noise tolerance and lower penalty than other CPE algorithm like VVPE and QPSK partitioning.

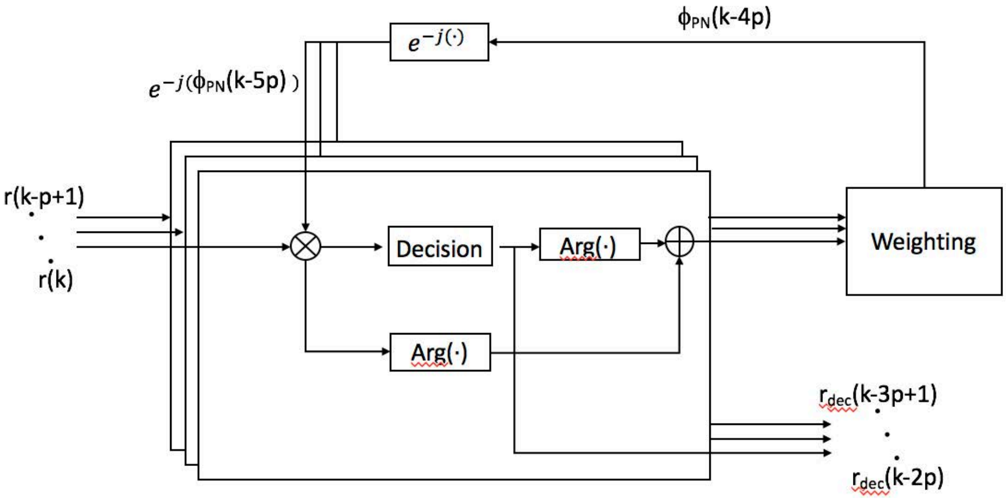

Fig. 3.11 Concept of parallelization

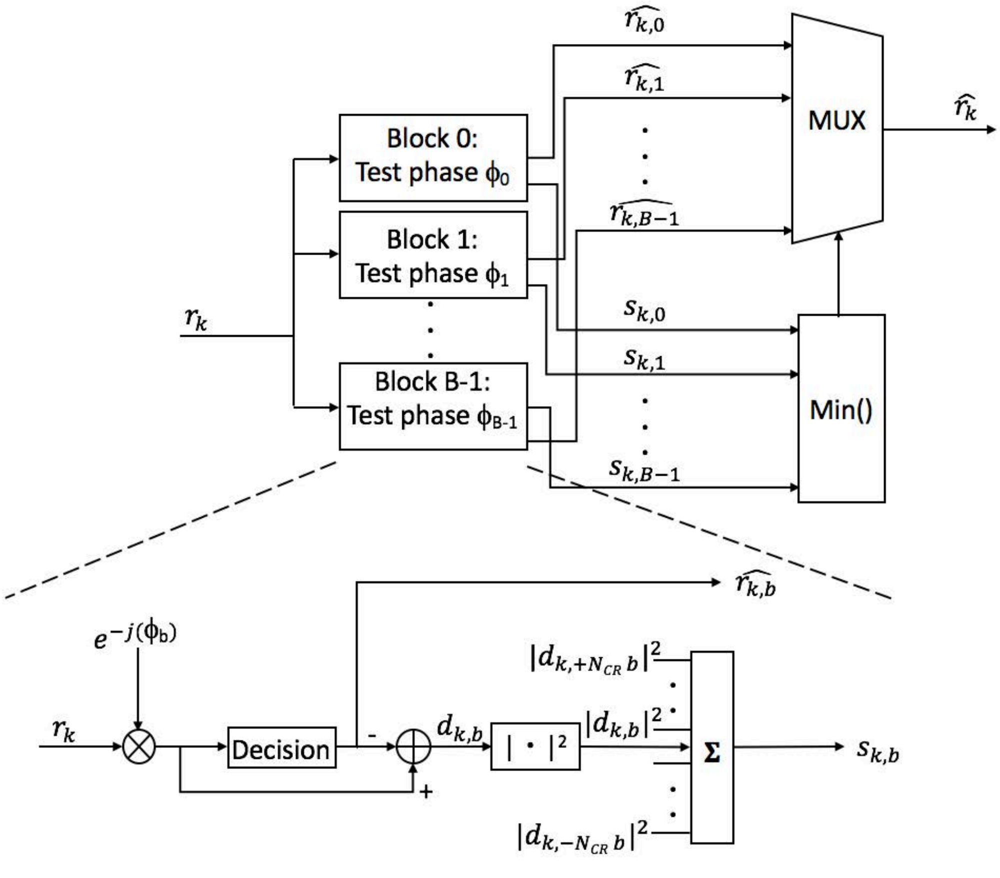

Fig. 3.12 Block diagram of BPS, showing the estimation of LPN

Chapter 4

Single Carrier Transmission with Multiple Independent Lasers

4.1 Introduction

High symbol rate single carrier signal for Tb/s transmission has become a popular research in coherent optical communication recently. However, as mentioned in previous sections, bandwidth provided by opto-electronics components had been a hurdle for further development and researchers needed to develop novel approaches to overcome this limitation. Besides ETDM and OTDM methods to generate single carrier signal [15] [70] [71], spectral slicing techniques is another way to generate single carrier signal with high symbol rate. With a set of carriers of different frequencies and modulators, a large bandwidth signal was first sliced into multiple pieces, modulated separately and eventually combined precisely at transmitter output. When signal was received in receiver end, it could be treated as a wide bandwidth signal from a single carrier, thus this approach named single carrier transmission.

To perform precise mixing of sub-bands at transmitter, optical frequency comb generator [7] [72] [73] was often used to generate set of carriers with uniform frequency spacing and locked phase. However, some architecture of the proposed frequency comb generator was not so attractive for practical use yet, based on the stability and flatness requirement for commercial communication systems.

To tackle drawbacks of optical comb generators, we are proposing a new transmitter architecture for single carrier transmission, which replace the comb generator with a set of independent lasers with different lasing frequencies. Recently, commercially available lasers are possessing Lorentzian linewidth of 50 to 200 kHz generally and keep improving over years.

With our proposed frequency offset estimation technique, as well as conventional CMA and CPE, FO of each laser could be compensated to an acceptable level for transmission.

4.2 Operating principle

Consider a transmitter employing spectral slicing technique to generate single carrier signal, but using multiple independent lasers instead of single laser with an optical frequency comb generator, as shown in figure 4.1. Given that multiple independent lasers were used to replace the conventional setup, MZM modulator for frequency combs generation and de-multiplexer for carrier separation was no longer required. Assume s(t) be the generated high symbol rate single carrier signal, which possessed an overall bandwidth of B, corresponding spectrum of s(t), S(f), was first sliced into K sub-bands, hence producing $S_1(f)$, $S_2(f)$, …, $S_K(f)$. Time domain counterpart of these sub-bands $s_k(t)$ were used for modulating the k^{th} laser.

To avoid overlapping of sub-bands during mixing, lasing frequency intervals of lasers were set to be B/K Hz. Furthermore, independent lasers were applied to replace single laser and the comb generator, thus each of these lasers should possess statistically independent LPN $\phi_1(t), \phi_2(t), \dots, \phi_K(t)$ and constant

FO $\Delta f_1, \Delta f_2, \ldots, \Delta f_K$. Hence, the generated high baud rate signal could be expressed as follow:

$$\boldsymbol{s(t)} = \sum\nolimits_{k=1}^{K} \boldsymbol{s_k(t)} \cdot \boldsymbol{e^{j2\pi(\frac{k}{K}B)t}} \cdot \boldsymbol{e^{j(2\pi\Delta f_k+\phi_k(t))}} \qquad \mathbf{(4.1)}$$

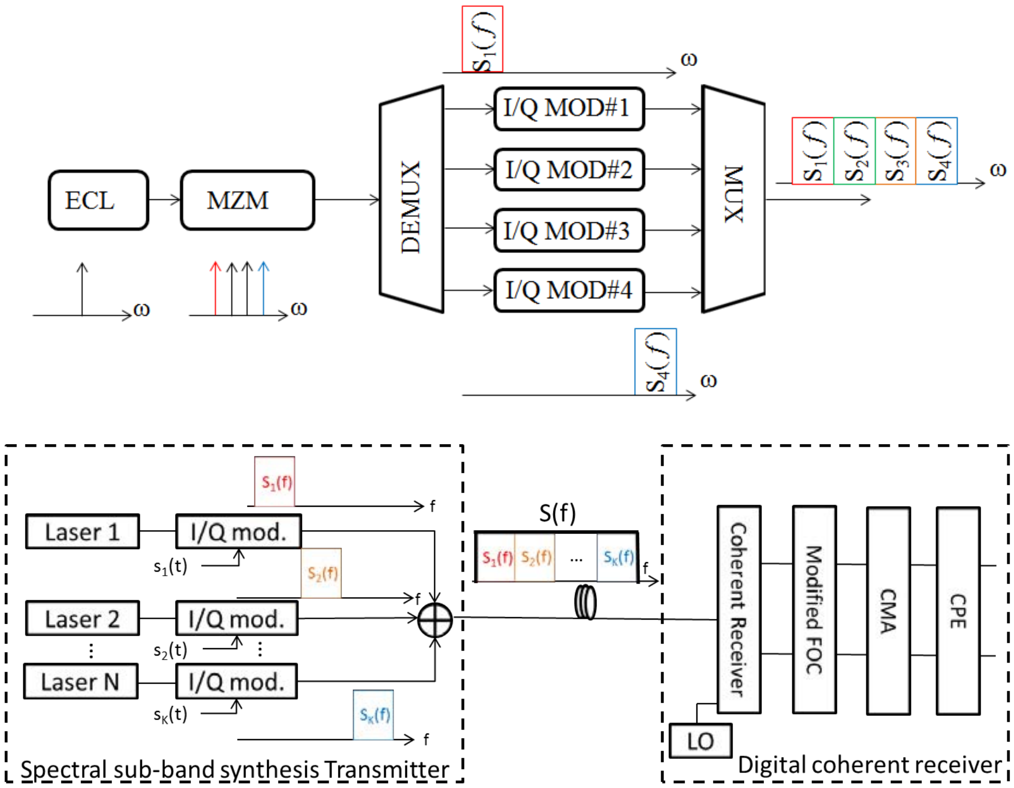

Fig. 4.1 Comparison of spectral slicing transmitter architecture. Up: Conventional spectral slicing transmitter configuration; Down: Proposed spectral slicing configuration and receiver DSP blocks for spectral sub-band synthesis using multiple independent lasers.

As mentioned in section 2, presence of LPN in conventional coherent communication system could be treated as a unitary rotation on symbols of corresponding format, leading to change in argument between original and received symbol. In our proposed configuration, multiple lasers and modulators were employed. Each transmitted symbol is made up of K vectors, which do not belong to any modulation format and have no any default constellation points for any generated symbols. Thus, each of these symbol's component from different sub-band will suffer a unitary rotation, where rotation on each sub-band's component is statistically independent. Figure 4.2 showed the evolution of phase noise in a 2-band transmission system. As observed, initial phase noise for sub-conventional coherent system, as phase between two lasers were not synchronized.

Figure 4.3 comparing behavior of LPN towards (a) Conventional coherent communication, and (b) Spectral slicing technique with multiple independent lasers. In the proposed setup, the entire signal spectrum was divided into parts, depending on lasers used. Passing through corresponding MZM and vector components of different modulus were generated due to equal division of overall spectrum bandwidth. Independent LPN from lasers will contribute to unique rotation angles in vector components. When components were added up in transmitter output, the resultant vector is no longer suffering from a constant modulus rotation, common distortion in conventional coherent communication, but a two-dimensional dispersion instead.

As vector components from modulators' output do not fall into any modulation format like QPSK or 16QAM, CPE needed to be applied to overall received symbol instead of each vector components. In our configuration, symbols were made up of multiple vectors, where each of them suffered from corresponding distortions including LPN and FO, received symbols will receive a two-dimensional distortion even ASE noise was not considered, which could be observed in figure 4.3(b).

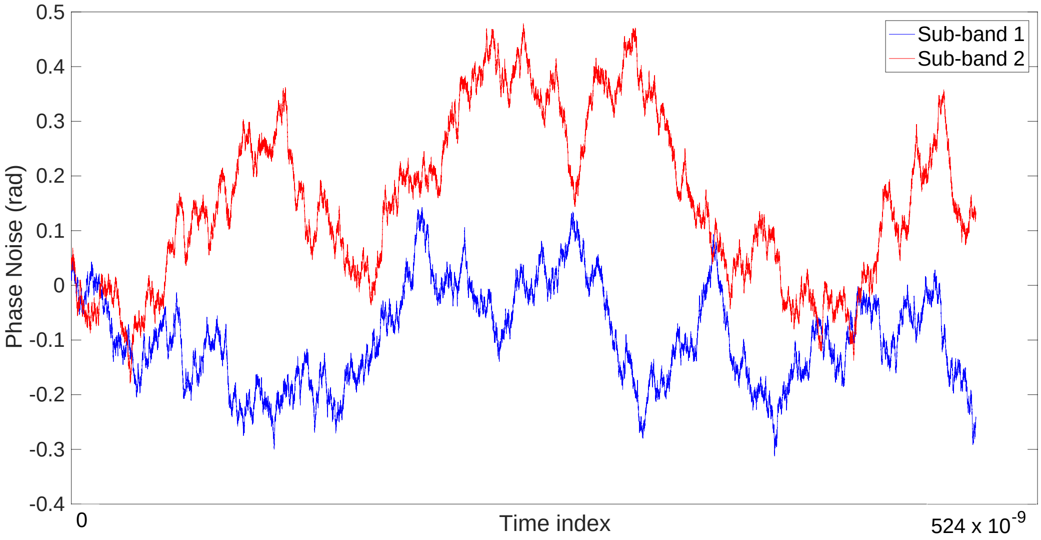

Fig. 4.2 Evolution of LPN in a 2-band communication system

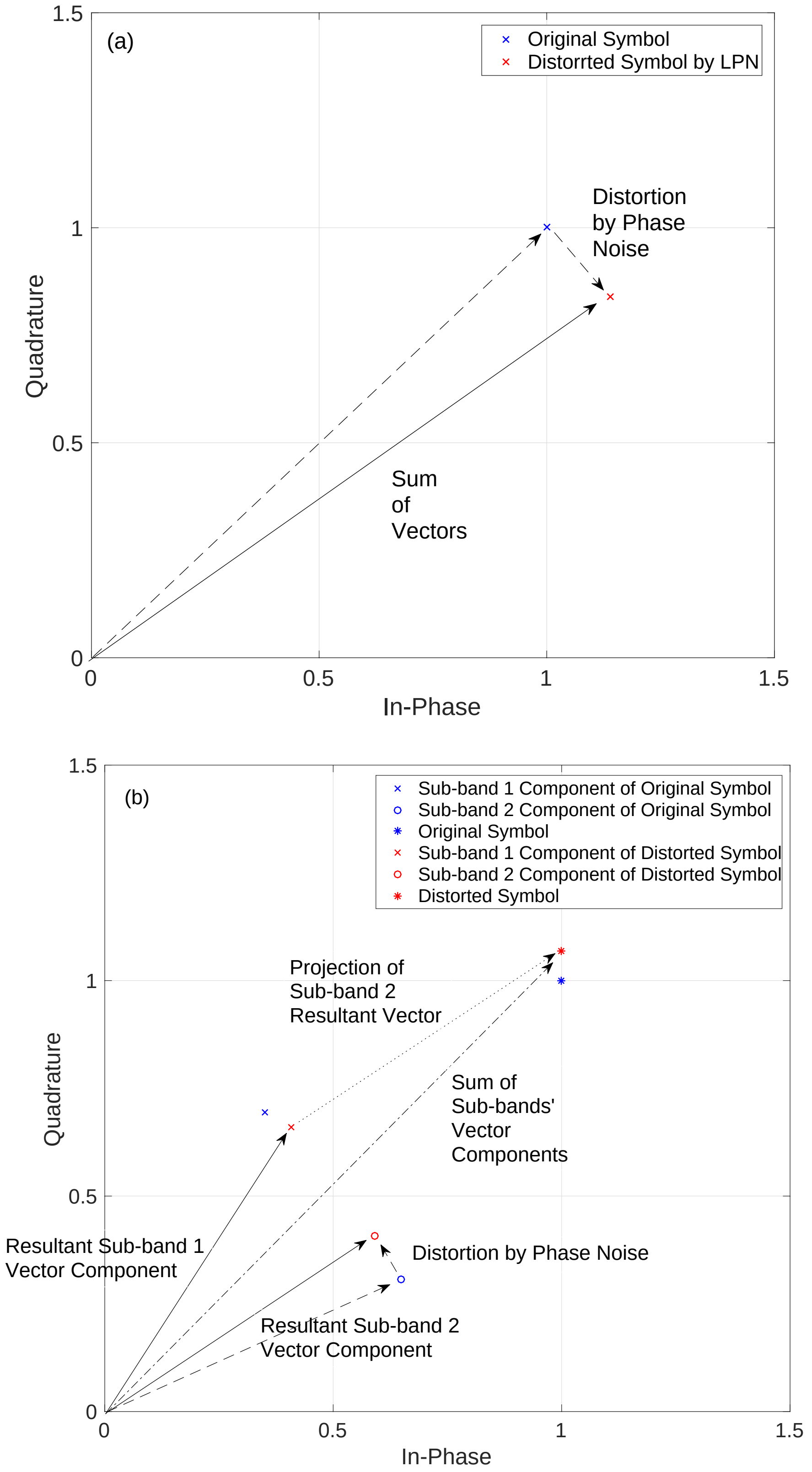

Fig. 4.3 Distortion of LPN on symbols in (a) Conventional coherent communication, and (b) Proposed spectral slicing configuration with 2 independent lasers

Figure 4.4 shows the distortion of original symbols, under presence of laser phase noise in transmitter end. The constellation plot showing a “tail” and a “head” in each QPSK region. A “tail” would be found with similar phase noise in all sub-bands, while a “head” could be found when phase noise in sub-bands did not agree. The tail part behaves similarly to unitary rotation in symbols, which was found in single band transmission. The head part behaves similarly to AWGN channel, where random vector was added to original symbols, causing symbols to leave the constant modulus circle. The head part of symbols implying a hypothesis that symbols dispersing from the constant modulus circle is inevitable in this proposed architecture, even with high OSNR. Degree of such dispersion depends on number of sub-bands, laser linewidth and baud rate.

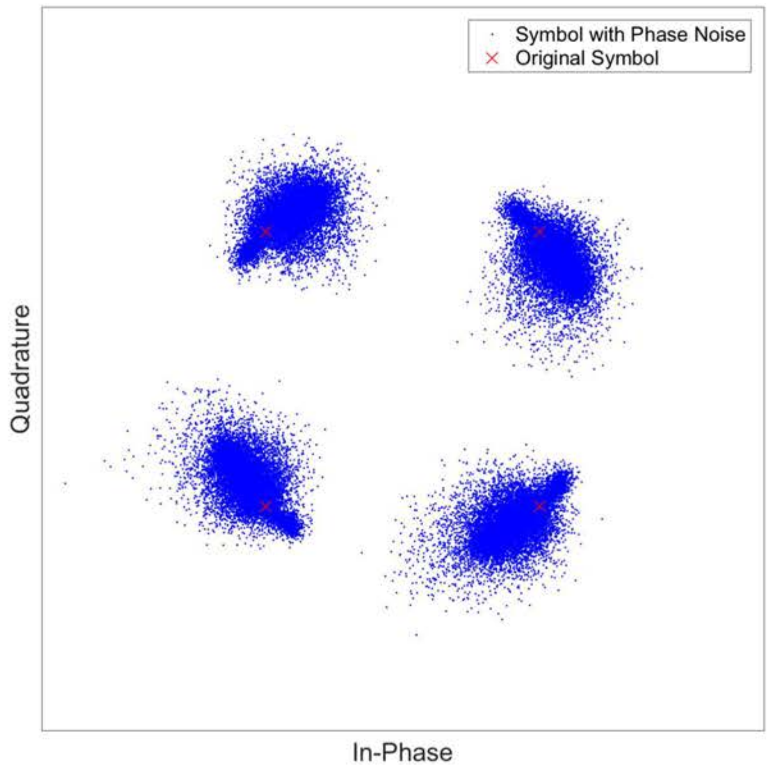

Fig. 4.4 Comparison of original symbols and received symbols, in a 2-bands QPSK system, under LPN distortion. ASE noise and receiver LPN were absent. Laser linewidth of sub-bands were set to 100 kHz.

As discussed in chapter 2, FO is also an important distortion besides LPN which also cause rotations to symbols. However, the major difference is that FO totally depends on frequency mismatch between transmitter and receiver, while LPN follows Wiener process and behaved in a random manner. Comparing figure 2.2 and 2.4, one may observed FO may induced larger phase rotation, or greater distortion, on transmitted symbols. Hence, we may expect FO will also contribute to larger proportion of distortion of symbols in our proposed configuration.

Each transmitted symbol of certain modulation format is composed of K vectors of different modulus without any format. Consider a long stream of data, where symbols suffered from FO will rotate around 2π. Given symbols were made up of multiple smaller vectors in our proposed architecture, compared to conventional coherent optical system, each of these small vector components will rotate by 2π. When these distorted vectors were added together at transmitter output, symbols will further disperse from the original designated point, as shown in figure 4.5, as if transmitting with very low OSNR.

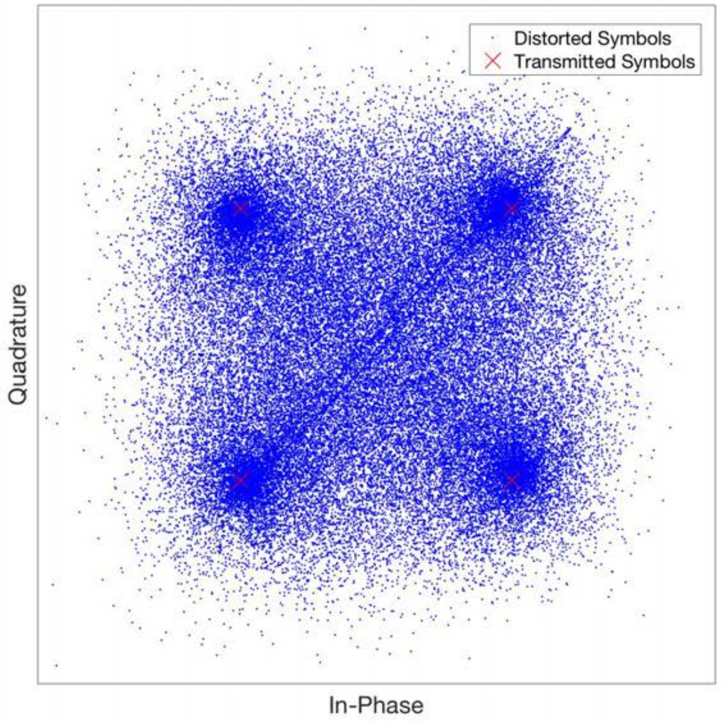

Fig. 4.5 Comparison of original symbols and transmitted symbols, in a 2-bands QPSK system, under FO distortion with 500MHz at each band and overall bit rate of 125GBaud. ASE noise and all LPN were absent.

Comparing figure 4.4 and 4.5, one may spot FO induced greater distortion to symbols than LPN, which could be explained through investigating signal spectrum in figure 4.6. The exponential term in time domain equaled to shift in frequency in frequency domain. Compared to $e^{-j\phi(t)}$, $e^{-j2\pi\Delta f t}$ brought larger shift in frequency for most cases, hence FO contributes more for frequency mismatch in receiver side. Moreover, given that sub-bands were suffering independent FO in transmitter and may shift in random direction, one should also consider inter-carrier interference between sub-bands as no spaces were left between sub-bands, where the overlapped part was added up together and further distorted transmitted signal.

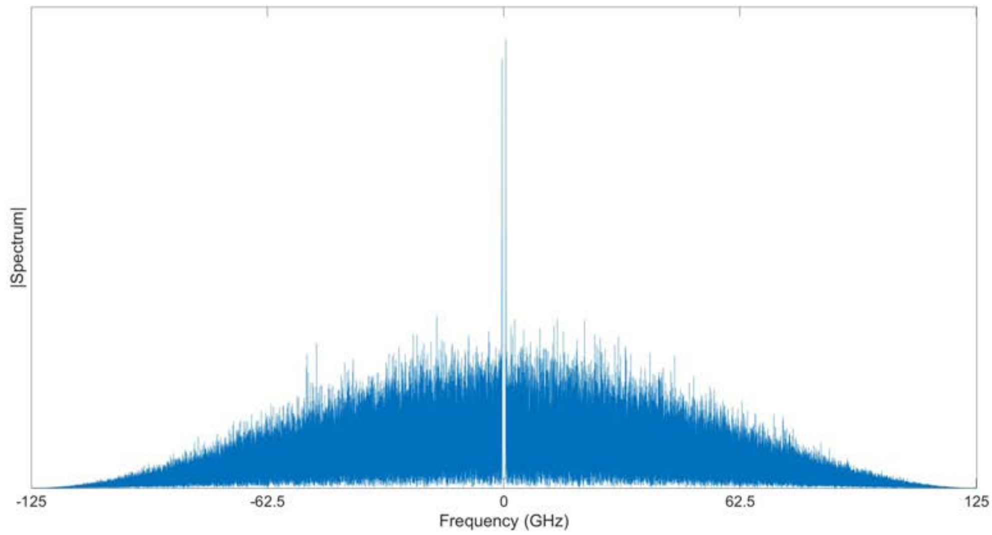

Fig. 4.6 Transmitted spectrum of 2 band system with proposed configuration. FO of each band was set to 500 MHz away from the adjacent band, LPN and ASE noise were absent for clarity.

4.3 Digital signal processing platform (DSP Platform)

4.3.1 Without frequency offset

In previous session, symbol distortions under single or multi independent lasers and corresponding proposed DSP platform were discussed. For better illustration, it would be better to investigate the whole configuration in multiple steps. With absence of FO, received signal were assumed to have undergone CD, I/Q imbalance, de-skew and retiming compensation. According to our proposed DSP platform, received symbols were passed directly to the CMA filter. CMA filter is a blind, format independent numerical DSP algorithm, which equalizes signal through following the constant modulus criterion to mimic the channel response and compensate distortions with inverse of channel response. In our proposed setup, a 101-tap CMA filter was employed to treat distorted signal. Figure 4.7 shows the signal constellation before and after filter's convergence for

125 GBaud PM-QPSK and PM-16QAM signals, where they were synthesized from different number of independent lasers. Linewidth of each laser was set to 100kHz, and ASE noise was absent from the simulation. The CMA filter was considered to function effectively as received symbol's constellation distributions were improved in most of the cases, except for the single band PM-16-QAM signal as CMA was not optimized for it. Furthermore, such result could be explained as other than polarization de-multiplexing, CMA filter could also be used for exerting various phase shift to each sub-band, in attempt to synchronize each lasers' phase across the entire signal spectrum.

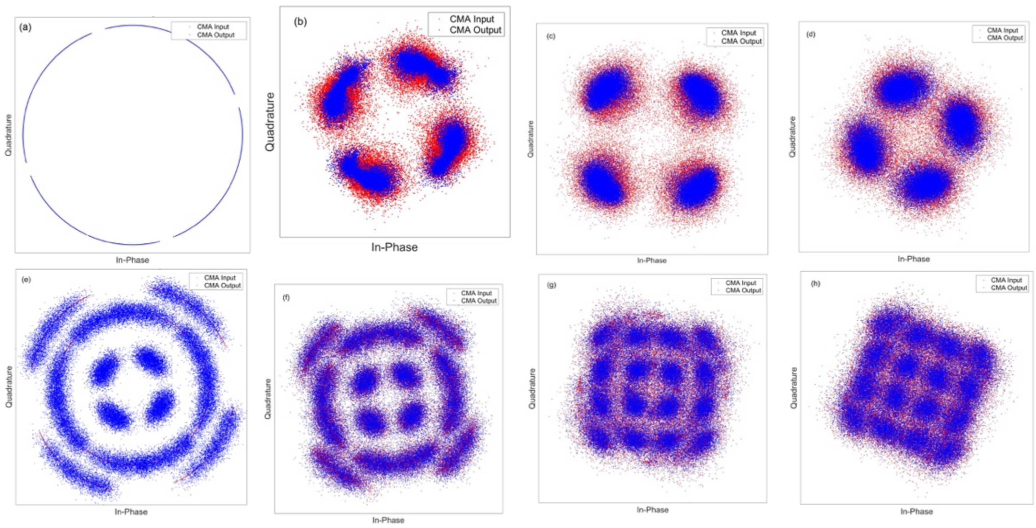

Fig. 4.7 Received signal distributions before and after CMA for 125 GBaud PM-QPSK signals synthesized from (a) 1 sub-band (b) 2 sub-bands (c) 4 sub-bands and (d) 8 sub-bands and received signal distributions before and after CMA for 125 GBaud PM-16-QAM signals synthesized from (e) 1 sub-band (f) 2 sub-bands (g) 4 sub-bands and (h) 8 sub-bands. The laser linewidth is 100 kHz and no laser frequency offsets and ASE noise are present.

To further investigate performance of the CMA filter on both PM-QPSK and PM-16-QAM signal, evolution of CMA filter cost function and resulting bit – error ratio (BER) against OSNR were plot and shown in figure 4.8 for 125 GBaud

PM-QPSK and PM-16QAM signals, with BPS applied as CPE after CMA convergence. In figure 4.8 (a), Cost function of 125 GBaud PM-QPSK signal synthesized from 2, 4 and 8 bands were compared. Determining from the shape and change in cost function, more iterations were required for CMA filter to converge for signal synthesized from more independent lasers, which matched our expectations as more time was required to align all the laser phase if more lasers were used. Given complexity of signal increased with more sub-bands, it is more difficult for CMA filter to align numerous lasers’ phase. Hence, the cost function at convergence is higher with more sub-bands used, indicating a better constellation distribution improvement at CMA convergence with less number of lasers.

Figure 4.8 (b) and (c) investigated the relation between number of sub-bands and corresponding performance with different modulation format, without influence of frequency offset. 65536 PRBS was transmitted under double sampling. As stated in figure 4.8 (a), as increasing number of sub-bands also indicating increasing difficulty in laser phase alignment of each sub-band, leading to increasing OSNR penalty with increasing number of sub-bands, which valid for both QPSK and 16-QAM format. For QPSK signal synthesized by less lasers, like 2 bands QPSK signal, linewidth contributed negligible OSNR penalty compared to penalty due to multiple lasers configuration. However, as the system become more complex, contribution to OSNR penalty by laser linewidth become considerable, which was found more noticing when format was switched from QPSK to 16-QAM, having more stringent requirement on number of sub-bands and linewidth of each independent laser.

When 16-QAM was used as modulation format for synthesized signal, OSNR penalty between setups under same laser linewidth slightly increased (About 0.5 and 1dB at BER = 1e-3 for QPSK and 16-QAM, with 50kHz laser linewidth), but still acceptable. However, if 100 kHz laser linewidth was adopted in all lasers, one may notice system performance degraded drastically with increasing number of lasers. 16-QAM signal synthesized by 2 lasers of 100 kHz reach the threshold of 2e-2 at around 26.5 dB, with about 1.5 dB penalty compared to its single band theoretical setup, which also reached a BER floor at around log(BER) = -2.2517.

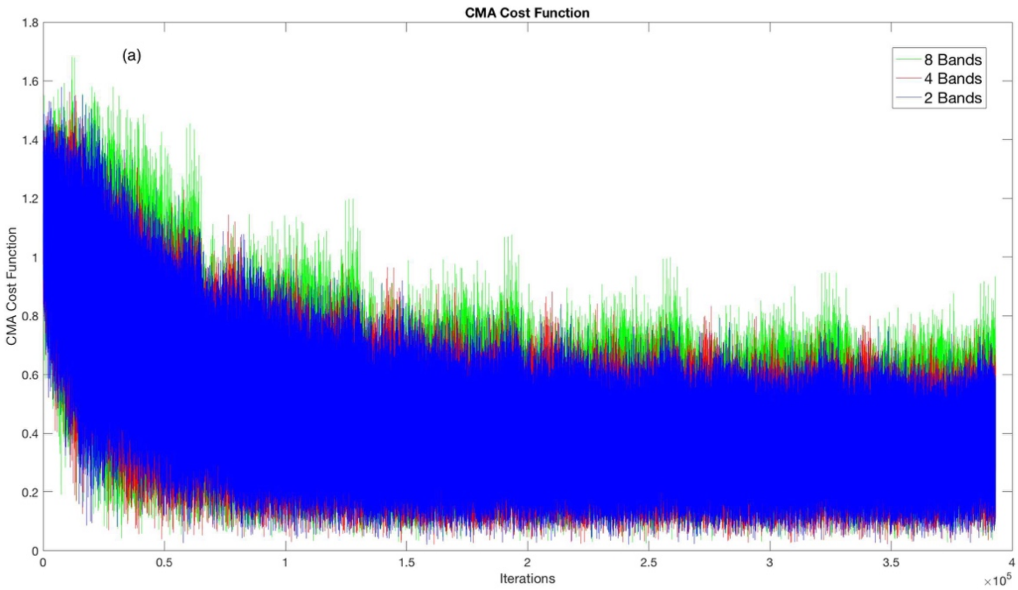

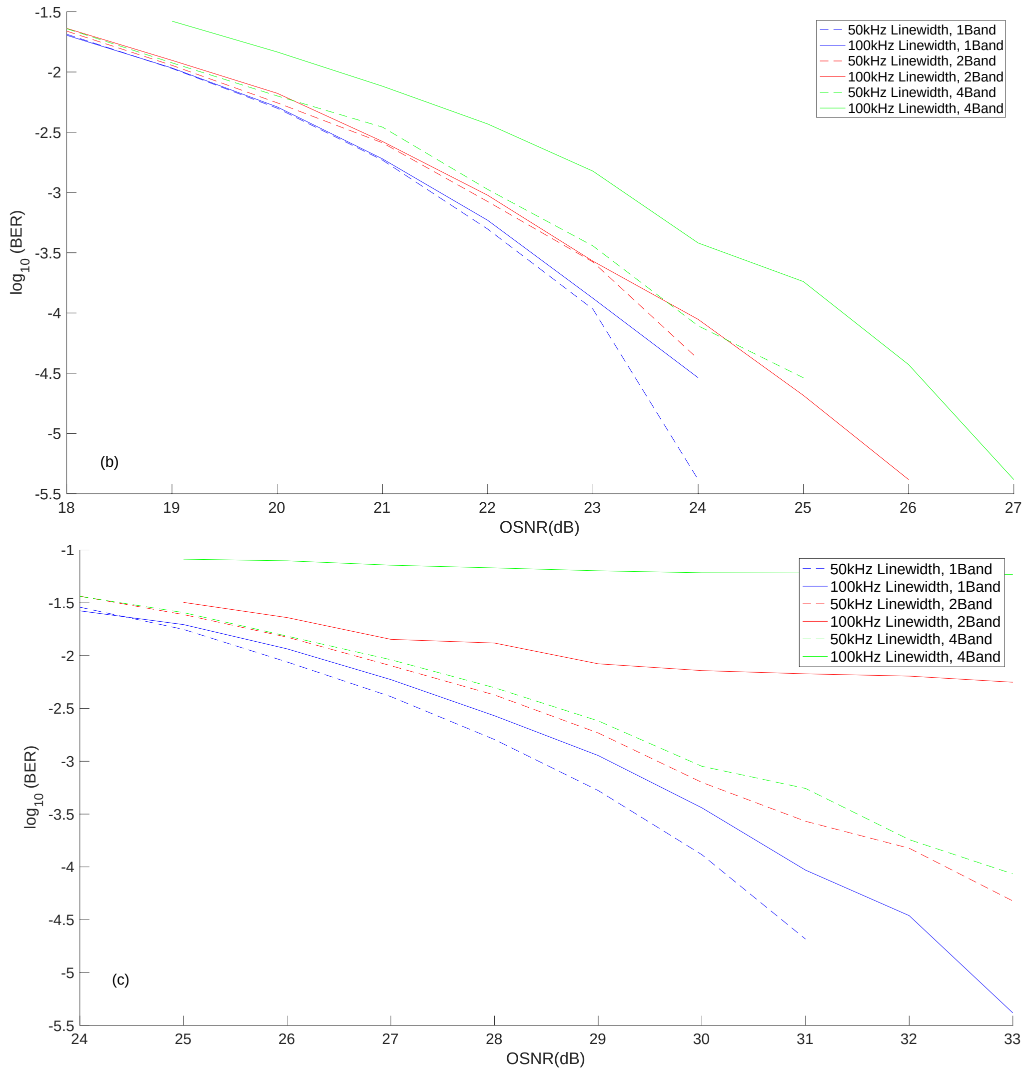

Fig. 4.8 (a) CMA Cost function for 125 GBaud PM-QPSK signals synthesized from 2, 4 and 8 sub-bands; BER vs. OSNR for (b) 125 GBaud PM-QPSK and (c) 125 GBaud PM-16QAM signals synthesized by various number of sub-bands with various levels of linewidth.

Based on these figures, we showed proposed configuration performance related to three major factors, they are system complexity (number of sub-bands), laser linewidth and modulation format. As happened in conventional coherent optical transmission, advanced modulation format usually provides higher symbol rate, but also require better hardware. Increasing number of sub-bands may allowed user to maintain same symbol rate with lower cost DACs, at the expense of larger OSNR penalty due to increasing difficulty in laser phase alignment for all sub-band lasers at CMA filter convergence. Although laser linewidth did not show any direct impact on system performance, through lower the variance of instantaneous phase noise and suppressed LPN increment, better laser phase alignment could be achieved after CMA filter convergence, and eventually improved system performance by reducing OSNR penalty, which is critical for realistic application usually having a tight power budget. Although 50 kHz lasers were used in simulation, it is still acceptable as there are 50kHz ECLs available on market already [74].

4.3.2 With frequency offset

Given the difficulty in recovering distorted signal under effect of FO and LPN, a pilot-aided frequency offset compensation algorithm was proposed, with corresponding block diagram shown in figure 4.9. Assuming symbols had undergone CD, I/Q imbalance and de-skew compensation, signal will first be passed to FOE, followed by CMA and BPS as CPE.

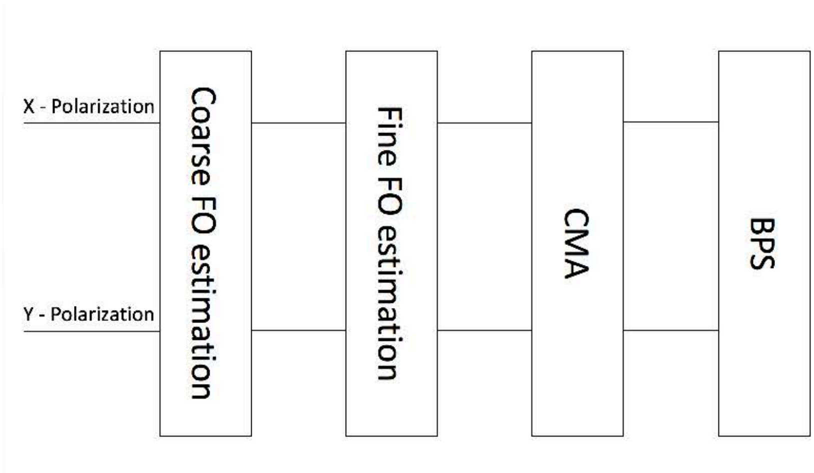

Fig. 4.9 Block diagram of proposed DSP platform at receiver end

The proposed FOE algorithm was developed based on the idea by Zhao [46]. Zhao's idea exploited characteristics of time-frequency domain transformation. As shown in figure 3.6 and 3.7, a designated constellation point of certain format was selected, take 1+1j in QPSK format for example. A stream of designated point was sent repeatedly, acting as pilot symbols, with padded zeros inserted between switching of pilot and payload to smoothen the process. By the nature of Fourier transform, a constant, steady stream of data possessed zero frequency and creating a spike at the baseband of signal spectrum. The spike acting as pilot tone for the spectrum and facilitated calculation of FO simply by observing distance shifted away from original carrier frequency. Making use of this idea, we applied it in our two-band transmission, with padded zeros removed. When sub-bands experienced FO and shifting away from original position, the spike at base band will move together will the rest of the signal spectrum, hence split into two pilot tones if the original one is sharp enough, one at each sub band as shown in figure 4.6.

Based on the basic principle above, we may modify and further developed data structure for spectral slicing single carrier transmission with more sub-bands, such as 4 bands. To achieve this, we first pick two pre-defined constellation point of certain modulation format, and generated it with an alternating pattern of half the baud rate. For example, a switching stream of 1+1j and 1-1j at 62.5 GHz was inserted as pilot for signal transmitted at 125 GBaud. As such, two pilot tones were formed at the position of $\pm$62.5 GHz and split into 4 pilot tones when FO shifted all four sub-bands.

However, the proposed configuration required stringent alignment of sub-bands position, or residual frequency offset. Figure 4.10 showed impact of different residual FOs toward processed signal. Consider a two bands system, even small amount of FO as 1MHz, which was considered as negligible and could be handled by conventional VVPE system in ordinary coherent optical system, may still distorted symbols greatly and causing bit error rate (BER) does not meet the threshold of 1e-3 or even 2e-2.

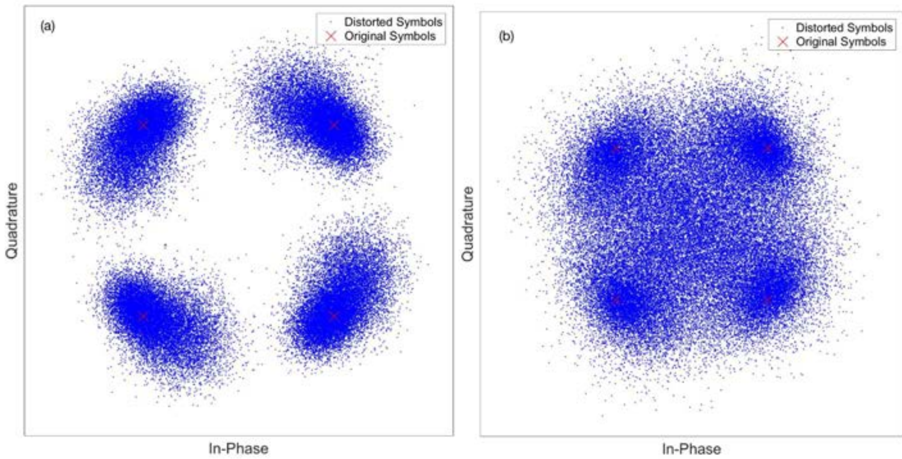

Fig. 4.10 Impact of residual of residual FO towards processed symbols: (a) 50kHz/sub-band; (b) 1MHz/sub band. OSNR and laser linewidth were set to 30dB and 100kHz respectively.

Considering a 125 GBaud system transmitting 2^{16} symbols at double sampling, frequency resolution df will be around 2MHz if signal undergoes a 2^{17} points discrete Fourier transform (DFT), is not enough for our proposed method to compensate FO to an acceptable level.

To solve the residual FO problem, we introduced application of error vector magnitude (EVM) in FO estimation. The first section of data stream was defined as pilot symbols, which were set to an arbitrary constellation point of the modulation format and known by receiver. Although does not follow any modulation format, we still knew pilot symbols’ vector components from sub-bands through performing fast Fourier transform (FFT) on pilot symbols and investigate each sub band signal. The following algorithm is based on the principle of maximum absolute error. Consider a coarse estimation of $\widehat{f_{k,coarse}}$ by finding shift in pilot tone in k^th sub band, the error of $\widehat{f_{k,coarse}}$ equaled to half of the frequency resolution df, which equals to:

$$df = \frac{baud\ rate}{N} \tag{4.2}$$

where N equaled to number of symbols transmitted.

Once df is known, one may found the true value of carrier frequency of sub band k $f_{k,coarse}$, lying within the range of $[\widehat{f_{k,coarse}} - 0.5df, \widehat{f_{k,coarse}} + 0.5df]$. Per accuracy needed, which based on number of sub bands or modulation format used, we can then set up fine steps within the range of $[\widehat{f_{k,coarse}} - 0.5df, \widehat{f_{k,coarse}} + 0.5df]$, creating a frequency test set like $A = [\widehat{f_{k,coarse}} - 0.5df, \widehat{f_{k,coarse}} - 0.25df, \widehat{f_{k,coarse}}, \widehat{f_{k,coarse}} + 0.25df, \widehat{f_{k,coarse}} + 0.5df]$, the simplest set available. Considering elements of A, the maximum absolute error was now decreased to 0.125 df, which is equivalent to 250kHz of FO between adjacent elements in our proposed setup.

With all frequency test sets were made, we could generate combinations of frequency sets for sub bands, where these sets were applied to sub bands in attempt to correct pilot symbols and calculate corresponding EVM, where the calculation of EVM is as follow:

$$\boldsymbol{EVM}(\%) = \sqrt[2]{\frac{\boldsymbol{P_{error}}}{\boldsymbol{P_{pilot}}}} \times \mathbf{100}\% \tag{4.3}$$

where P_{error} denoted average amplitude of error vector, while P_{pilot} is average amplitude of reference pilot symbol.

Consider a 2 bands QPSK system, with 1GHz FO at each band, the simplest frequency test sets A were established for each sub band. Testing EVM of corrected pilot symbols with combinations of FO, an EVM map was shown in figure 4.11. The closer the combination to the true FO is, the lower the EVM is. It is worth noticing that an EVM 'trough' is formed in a line near the true FO combination and maintaining a condition of:

$$|\widehat{\boldsymbol{f_{1,fine}}}| + |\widehat{\boldsymbol{f_{2,fine}}}| = |\boldsymbol{f_1}| + |\boldsymbol{f_2}| \qquad (\mathbf{4.4})$$

where $\widehat{f_{k,fine}}$ denoted the fine approximation FO of the k^{th} sub band from the proposed EVM approach. f_k denoted the true FO in the k^{th} sub-band.

If relation in equation 4.4 is maintained, resultant EVM will be kept at the trough position, which significantly lower than other adjacent points and stating the FOC solution need not to close to the true value. Solution other than exact FO values for sub bands could be viewed as successful recovery in the overall spectral shape with a small FO, which based on the step size of frequency test set, or frequency resolution fundamentally, in the overall spectrum.

Once the fine estimation of FO was done, positions of sub bands were recovered and in acceptable alignment in terms of spectral position. However, one should also consider distortions due to inter-carrier interference, which could not be recovered through FO estimation in the proposed algorithm as spectrum was already mixed up in transmitter. To alleviate distortion of symbols due to inter-carrier interference, we simply divided the overlapped part by $\sqrt{2}$, attempting to retrieve spectral power of the overlapped part. The slightly shifted spectrum was then passed to an accurate two stage FOC algorithm developed by Huang which was originally designed for conventional coherent optical system instead of spectral slicing transmitter [43]. After the two stage FOC, the residual FO at sub bands or FO in overall spectrum are both negligibly small, at the order of kHz, which did fall within the tolerance range of CPEs, implying CPEs will able to perform their own tasks and treat residual FO distortions as an additional phase noise on symbols.

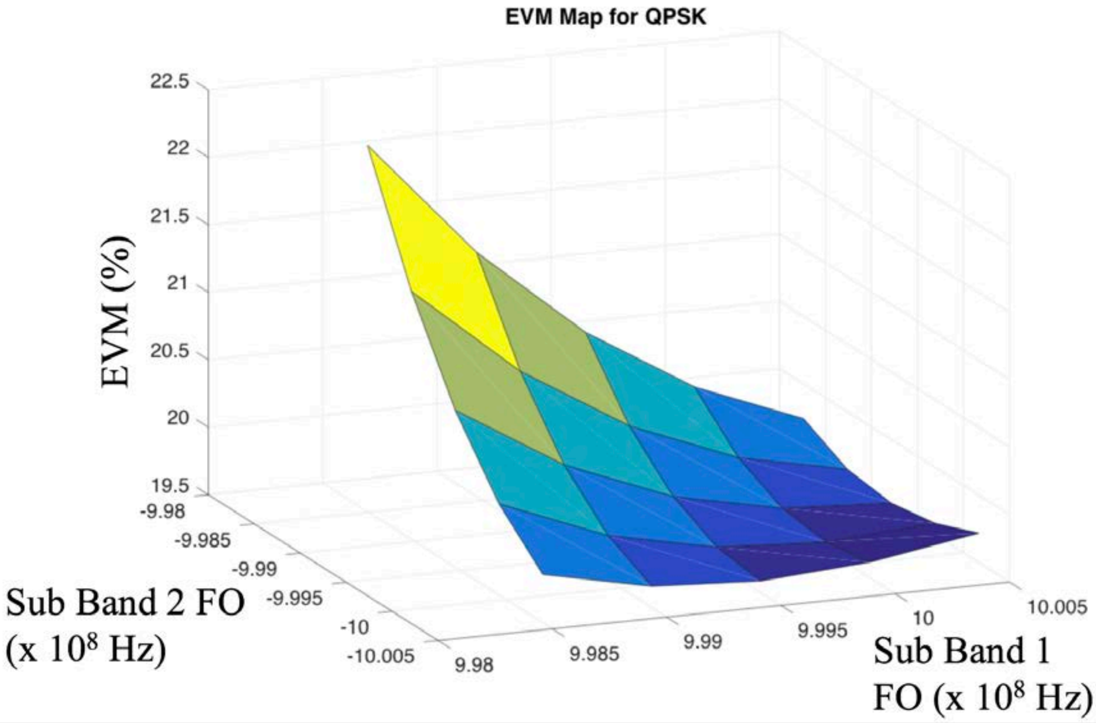

Fig. 4.11 EVM map of a 2 bands QPSK system. FOs were set as 1 GHz at each sub band, laser linewidth was set to 100kHz and ASE noise was included.

Proposed algorithm was applied in transmitting both PM-QPSK and PM-16-QAM signal with different configurations, including laser linewidth and FO in each sub-band. Performance of configurations were plot as BER curves and compared in figure 4.12, with two thresholds set at BER = 2e-2 and 1e-3 respectively.

Figure 4.12 (a) and (b) compared PM-QPSK system performance of different configuration with 50 and 100 kHz laser linewidth respectively, while 2 and 10% of pilot symbols were applied for 2 and 4 sub-band cases separately to maintain sharpness of pilot tones after suffering from frequency offset in each sub-band. For PM-QPSK system, the proposed approach showed negligible penalty at both threshold of BER = 2e-2 and 1e-3, except for those composed of 4 sub-bands with 100 kHz laser linewidth and the 2 sub-bands case with 100 kHz laser linewidth and 1 GHz FO in each sub-band. Simulation results showed such approach is feasible for PM-QPSK systems with up to 4 sub-bands and 1 GHz FO in each sub-band.

Figure 4.12 (c) showed performance of 2 sub-band PM-16-QAM system under various FO settings. Result showed system performance degraded largely when moving from PM-QPSK towards PM-16-QAM. Multi sub-band system never reach the threshold of 1e-3 and suffering from 1 and 2 dB penalty at the threshold of BER = 2e-2, when 500 MHz and 1 GHz FO were presented in each sub-band. The reason behind this degradation could be accounted to stringent requirement of noise compensation and the poorly compensated spectral portion which was overlapped with adjacent sub-band prior to FO compensation.

Although proposed configuration suffered from great degradation, result showed the proposed configuration able to perform single carrier transmission with multiple independent lasers.

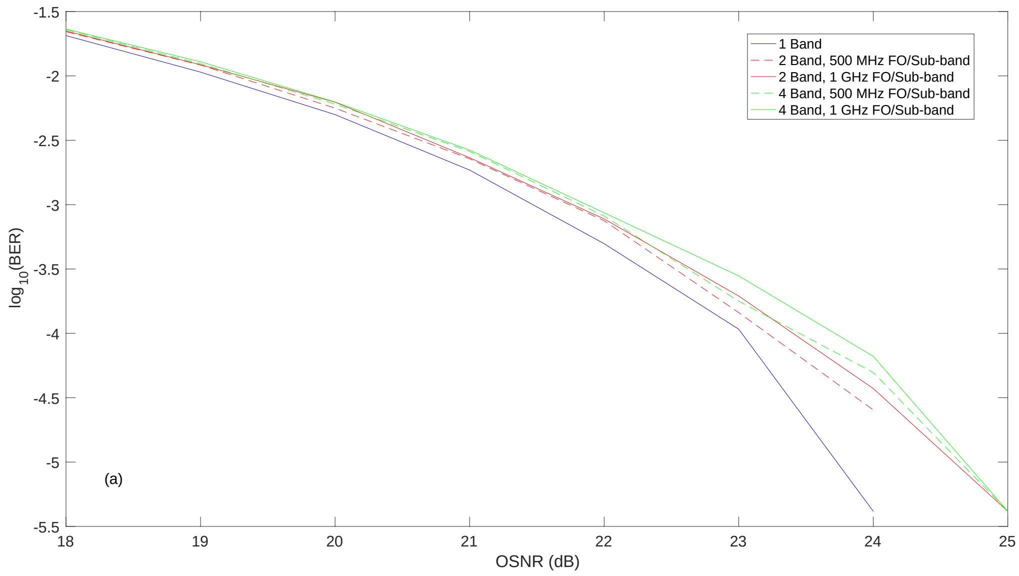
1 Band
2 Band, 500 MHz FO/Sub-band
2 Band, 1 GHz FO/Sub-band
4 Band, 500 MHz FO/Sub-band
4 Band, 1 GHz FO/Sub-band
(a)
log10(BER)
OSNR (dB)
-1.5
-2
-2.5
-3
-3.5
-4
-4.5
-5
-5.5
18
19
20
21
22
23
24
25

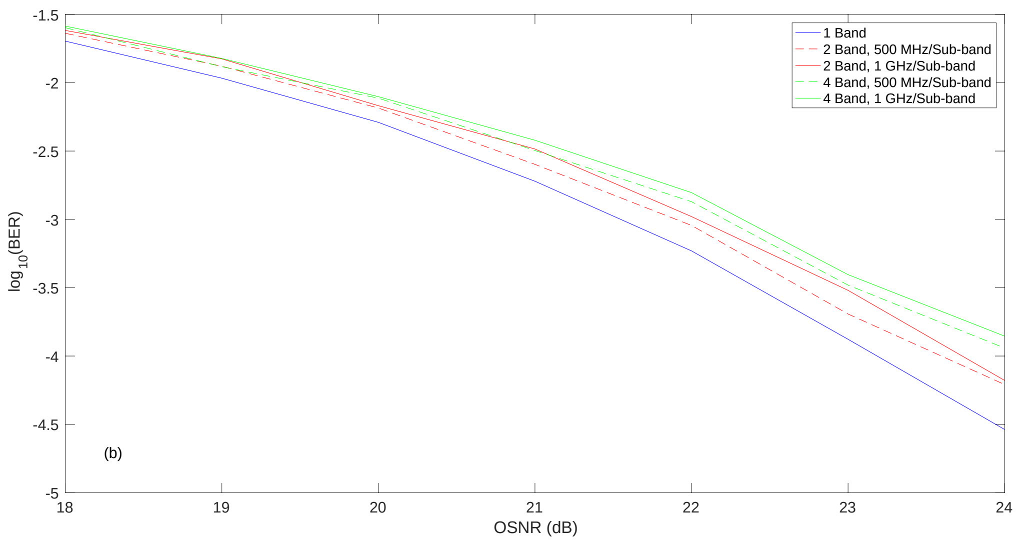
1 Band
2 Band, 500 MHz/Sub-band
2 Band, 1 GHz/Sub-band
4 Band, 500 MHz/Sub-band
4 Band, 1 GHz/Sub-band
(b)
log10(BER)
OSNR (dB)
-1.5
-2
-2.5
-3
-3.5
-4
-4.5
-5
18
19
20
21
22
23
24

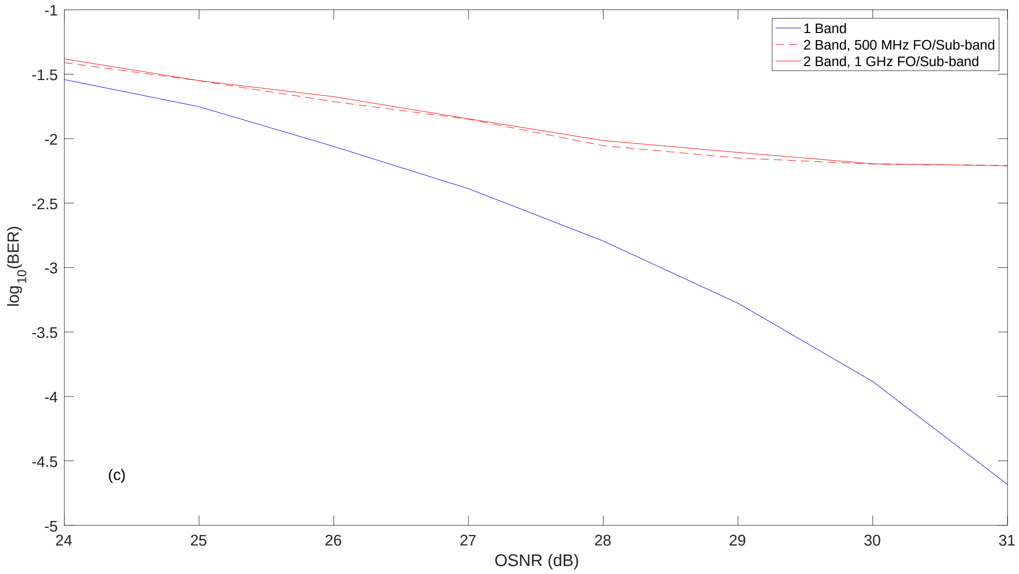

Fig. 4.12 BER performance of proposed configurations with different laser linewidths: (a) PM-QPSK signal with 50 kHz laser linewidth; (b) PM-QPSK signal with 100 kHz laser linewidth, and (c) PM-16-QAM signal with 50 kHz laser linewidth. BPS was used as the CPE.

Chapter 5

Conclusions and Future Directions

This thesis investigated major impairments in coherent communications and corresponding DSP algorithm for compensation. In addition, a transmitter configuration employed multiple independent lasers and modulators, which could achieve 1 Tb/s transmission, was proposed with a new DSP platform specifically designed for such configuration. The proposed platform was studied numerically to verify platform's performance, under different modulation format and impairments parameters, including FO and LPN.

Considering a coherent optical communication system, respective laser impairments like FO and LPN were studied in chapter 2. Through investigating how laser impairments distort signal transmission, importance of DSP algorithm was show essential for recovering symbols of various modulation formats.

Based on the understanding of laser impairments mentioned above, various DSP algorithms were introduced in chapter 3. These algorithms were proposed for compensating different origin of noise, thus their development and corresponding performance were discussed, showing pros and cons of each algorithm and realize suitable algorithms for our proposed configuration.

The proposed configuration of spectral slicing transmitter using multiple independent lasers was introduced in chapter 4. Such configuration was investigated mathematically and showing properties of distortions to be encountered. Investigations showed the transmitted symbols behaved as a summation of vectors with unequal energy distribution and unique rotation among vector components due to properties of spectral slicing and multiple independent lasers. FO also exhibits in lasers together with LPN, thus each sub-band contributing to vector components also suffered from a frequency shift in Fourier domain, and eventually may lead to non-alignment of sub-bands. To deal with sub-bands non-alignment, a receiver DSP platform was also proposed and investigated numerically, aiming to compensate symbol distortions to achieve the threshold of log10 (BER) = 1e-3 or 2e-2.

To end with, a spectral sliced transmitter using multiple independent lasers and a receiver DSP platform were proposed. 1 Tb/s transmission of PM-16-QAM signal was achieved with 2 sub-bands transmission at a penalty of about 1.5 db. Such configuration showed another approach to construct spectral slicing transmitter is possible, improved flexibility of traditional WDM system as well as benefitting software-defined transmissions.

In future, transmission performance of various modulation formats could be further studied. Moreover, improvement could be made on the algorithm retrieving the overlapped parts or sub-band alignment of receiver spectrum, as well as preserving current system performance with less pilot symbols.

Bibliography

[1] R. J. Essiambre and R. W. Tkach, "Capacity trends and limits of optical communication networks," *Proceedings of the IEEE,* vol. 100, no. 5, pp. 1035-1055, 2012.

[2] K. Kikuchi and T. Okoshi, "Chapter 1," in *Coherent Optical Communication Systems*, Tokyo, Japan, KTK Scientific Publisher, 1988.

[3] K. Kikuchi, "Fundamentals of Coherent Optical Fiber Communications," *Journal of Lightwave Technology,* vol. 34, no. 1, 2016.

[4] S. Tsukamoto, D. Ly-Gagnon, K. Katoh and K. Kikuchi, "Coherent demodulation of 40 Gbit/s Polarization-Multiplexed QPSK signals with 16-GHz spacing after 200 km transmission," in *Optical Fiber Communication Conference*, Anaheim, CA, USA, 2005.

[5] P. J. Winzer, "Spatial Multiplexing in Fiber Optics: The 10x scaling of metro/core capacities," *Bell Labs Tech. J.*, vol. 19, pp. 22-30, 2014.

[6] P. J. Winzer, "Spatial Multiplexing: The Next Frontier in Network Capacity Scaling," in *ECOC*, 2013.

[7] R. Rios-Muller, etal., "1 Terabit/s Net Data-Rate Transceiver Based on Single-Carrier Nyquist-Shaped 124 GBaud PDM-32QAM," in *OFC*, 2015.

[8] G. Raybon, etal., "160 GBaud Coherent Receiver based on 100GHz Bandwidth 240 GS/s Analog to Digital Conversion," in *OFC*, 2015.

[9] S. Randel, etal., "All Electeronically Flexibly Programmable 864 Gb/s Single Carrier PDM 64-QAM," in *OFC*, 2014.

[10] D. O. Otuya, etal., "Single Channel 1.92 Tbit/s, 64 QAM Coherent Orthogonal TDM Transmission of 160 Gbaud Optical Nyquist Pulses with 10.6 bit/s/Hz Spectral Efficiency," in *OFC*, 2015.

[11] K. Schuh, etal., "100 GSa/s BiCMOS DAC supporting 400 Gb/s dual channel transmission," in *ECOC*, 2016.

[12] G. Raybon, etal., "Single-carrier all-ETDM 1.08-Terabit/s line rate PDM-64-QAM transmitter using a high-speed 3-bit multiplexing DAC," in *IPC*, 2015.

[13] J. Zhang and J. Yu, "WDM Transmission of Twelve 960 Gb/s Channels based on 120 GBaud ETDM PDM16QAM over 1200-km TeraWave Fiber Link," in *OFC*, 2016.

[14] J. Zhang and J. Yu, "Generation and Transmission of High Symbol Rate Single Carrier Electronically Time-Division Multiplexing Signals," *IEEE Photonics Journal,* vol. 8, no. 2, April 2016.

[15] H. Yamazaki, etal., "Single-carrier 1-Tb/s PDM-16QAM transmission using high-speed InP MUX-DACs and an integrated OTDM modulator," *Optics Express,* vol. 23, no. 10, p. 12866, 2015.

[16] M. Nakazawa, etal., "1.28 T-bit/s-70 km OTDM Transmission using third- and fourth-order simultaneous dispersion compensation with a phase modulator," *Electronics Letters,* vol. 36, no. 24, 2000.

[17] P. J. Pupalaikis, "Digital Bandwidth Interleaving," 29 March 2005. [Online]. Available: http://downloads.deusm.com/designnews/4316-Digital_Bandwidth_Interleaving.pdf. [Accessed 16 July 2017].

[18] C. Schmidt, etal., "Enhancing the Bandwidth of DACs by Analog Bandwidth Interleaving," in *Broadband Coverage in Germany; 10. ITG-Symposium*, Berlin, 2016.

[19] P. Pupalaikis, "High speed arbitrary waveform generator". Patent US7,535,394, 19 May 2009.

[20] X. Chen, etal., "180-GBaud Nyquist Shaped Optical QPSK Generation Based on a 240-GSa/s 100-GHz Analog Bandwidth DAC," in *ACP*, 2016.

[21] Oclaro, "400G Lithium Niobate Modulator," 2017. [Online]. Available: www.oclaro.com/product/400g-lithium-niobate-modulator . [Accessed 17 June 2017].

[22] X. Chen, etal., "Characterization of electro-optic bandwidth of ultra-high speed modulators," in *OFC*, 2017.

[23] Y. Ogiso, "Ultra-High Bandwidth InP IQ Modulator with 1.5 V V?," in *ECOC*, 2016.

[24] H. Huang, etal., "Broadband Modulation Performance of 100-GHz EO MZMs," *Journal of Lightwave Technology,* vol. 30, no. 23, pp. 3647-3652, 2016.

[25] M. Chacinski, etal., "Monolithically Integrated 100 GHz DFB-TWEAM," *Journal of Lightwave Technology,* vol. 27, no. 16, pp. 3410-3415, 2009.

[26] C. Xiong, etal., "Experimental Demonstration of Ultra-Dense WDM-PON with Seven-Core MCF-Enabled Self-Homodyne Coherent Detection," *IEEE Photonics Journal,* vol. 9, no. 2, pp. 1-7, 2017.

[27] I. Morohashi, etal., "Frequency Measurement of Thz waves by Electro-Optic Sampling using Mach-Zehnder-modulator-based Flat Comb Generator," 2016.

[28] C. Henry, "Theory of the Phase Noise and Power Spectrum of a Single Mode Injection Laser," *J. Quantum Electron.,* vol. 19, pp. 1391-1397, 1983.

[29] M. Tur, B. Moslehi and J. W. Goodman, "Theory of Laser Phase Noise in Recirculating Fiber-Optic Delay Lines," *J. Lightwave Technol.*, vol. 3, pp. 20-31, 1985.

[30] W. Loh, F. J. O'Donell, J. J. Plant, M. A. Brattain, L. J. Missaggia and P. W. Juodawlkis, "Packaged, High-Power, Narrow-Linewidth Slab-Coupled Optical Waveguide External Cavity Laser (SCOWECL)," *IEEE Photonics Technology Letters,* vol. 23, no. 14, pp. 974-976, 2011.

[31] D. M. Bird, J. R. Armitage, R. Kashyap, R. M. A. Fatah and K. H. Cameron, "Narrow Line Semiconductor Laser using Fibre Grating," *Electron. Lett.*, vol. 27, pp. 1115-1116, 1991.

[32] D. Godard, "Self-recovering Equalization and Carrier Tracking in Two-dimensional Data Communication Systems," *IEEE Trans. Commun.*, vol. 28, no. 11, pp. 1867-1875.

[33] S. Haykin, Adaptive Filter Theory, Englewood Cliffs, NJ: Prentice-Hall, 2001.

[34] S. J. Savory, "Digital Filters for Coherent Optical Receivers," *Optics Express*, vol. 16, no. 2, pp. 804-817, 2008.

[35] "ECL Lasers," [Online]. Available: https://www.thorlabs.com/newgrouppage9.cfm?objectgroup_id=4757. [Accessed 16 June 2017].

[36] D. Rife and R. R. Boorstyn, "Single Tone Parameter Estimation from Discrete-time Observations," *IEEE Trans. Inf. Theory*, vol. 20, no. 5, pp. 591-598, 1974.

[37] S. Kay, "A Fast and Accurate Single Frequency Estimator," *IEEE Trans. on ASSP*, vol. 37, no. 12, pp. 1987-1990, 1989.

[38] L. M. D. Le, K. C. Teh and K. H. Li, "Jammin Rejection using FFH/MFSK ML Receiver over Fading Channels with the Presence of Timing and Frequency Offsets," *IEEE Transactions on Information Forensics and Security*, vol. 8, no. 7, pp. 1195-1200, 2013.

[39] M. Moeneclaey, etal., "ML-Oriented NDA Carrier Synchronization for General Rotationally Symmetric Signal Constellations," *IEEE Tranactions on Communications,* vol. 42, no. 8, pp. 2531-2533, 1994.

[40] M. Rice, "Data-Aided and Non-Data-Aided Maximum Likelihood SNR Estimatiors for CPM," *IEEE Transactions on Communications,* vol. 63, no. 11, pp. 4244-4253, 2015.

[41] M. Pedzisz and A. Coatanhay, "Minimum Entropy Approach for Carrier Frequency Recovery," *IEEE Transactions on Wireless Communications,* vol. 5, no. 4, pp. 774-778, 2006.

[42] A. Leven, N. Kaneda, U.-V. Koc, and Y.-K. Chen, “Frequency Estimation in Intradyne Reception,” IEEE Photonics Technology Letters, vol. 19, no. 6, pp. 366–368, 2007.

[43] H. Dezhao, C. Tee-Hiang and C. Yu, "Accurate Two-Stage Frequency Offset Estimation for Coherent Optical Systems," *IEEE Photonics Technology Letters,* vol. 25, no. 2, pp. 179-182, 2013.

[44] J. C. M. Diniz, J. C. R. F. d. Oliveira, E. S. Rosa, V. B. Ribeiro, V. E. S. Parahyba, R. d. Silva, E. P. d. Silva, L. H. H. d. Carvalho, A. F. Herbster and A. C. Bordonalli, "Simple feed-forward wide-range frequency offfset estimator for optical coherent recievers," *Opt. Express,* vol. 19, no. 26, pp. 323-328, 2011.

[45] Y. Gao, A. P. T. Lau and C. Lu, "Residual Carrier-Aided Frequency Offset Estimation for Square 16-QAM Systems," in

OptoElectronics and Communication Conference held jointly with 2013 International Conference on Photonics in Switching, 2013.

[46] D. Zhao, etal., "Digital Pilot Aided Carrier Frequency Offset Estimation for Coherent Optical Transmission Systems," *Optics Express*, vol. 23, no. 19, pp. 24822-24832, 2015.

[47] J. R. Barry and J. M. Kahn, "Carrier Synchronization for Homodyne and Heterodyne Detection of Optical Quadriphase-shift keying," *J. Lightwave Technol.*, vol. 10, pp. 1939-1951, 1992.

[48] A. J. Viterbi and A. N. Viterbi, "Nonlinear estimation of PSK-modulated carrier phase with application to burst digital transmission," *IEEE Trans. Inf. Theory*, vol. 29, no. 4, pp. 543-551, 1983.

[49] K. P. Zhong, J. H. Ke, Y. Gao and J. C. Cartledge, "Linewidth-Tolerant and. Low-Complexity Two-Stage Carrier Phase Estimation Based on Modified QPSK Partitioning for Dual-Polarization 16-QAM Systems," *Journal of Lightwave Technology*, vol. 3, no. 1, pp. 50-57, 2013.

[50] C. Yin and H. Xu Guang, "A Linewidth-Tolerant Two-Stage CPE Using a New QPSK-Partitioning Approach and an Enhanced Maximum Likelihood Detection for 64-QAM Coherent Optical Systems," *Journal of Lightwave Technology*, vol. 33, no. 18, pp. 3883-3889, 2015.

[51] T. Shu, Y. Li, S. Fan, M. Yu, J. Pang, D. Kong and J. Wu, "Improved Amplitude and Phase Noise Mitigation for 16QAM

Transmission Using Viterbi-Viterbi Phase Estimator Combined with Extended Kalman Filter," in *ACP*, 2016.

[52] J. Han, W. Li, L. Huang, H. Li, Q. Hu and S. Yu, "Carrier Phase Estimation Based on Error Function Calculation for 16-QAM Systems," *IEEE Photonics Technology Letters,* vol. 28, no. 22, pp. 2561-2564, 2016.

[53] A. J. Stark, Y.-T. Hseuh, T. F. Detwiler, M. M. Filer, S. Tibuleac and S. E. Ralph, "System Performance Prediction with the Gaussian noise model in 100G PDM-QPSK coherent optical networks," *Journal of Lightwave Technology,* vol. 31, no. 21, pp. 3352-3360, 2013.

[54] I. Fatadin, D. Ives and S. J. Savory, "Laser Linewidth Toerance for 16-QAM Coherent Optical Systems using QPSK Partitioning," *IEEE Photon. Technol. Lett.,* vol. 22, no. 9, pp. 631-633, 2010.

[55] Y. Gao, A. P. T. Lau, S. Yan and C. Lu, "Low-Complexity and Phase Noise Tolerant Carrier Phase Estimation for Dual-Polarization 16-QAM Systems," *Optics Express,* vol. 19, no. 22, pp. 21717-21729, 2011.

[56] I. Fatadin, D. Ives and S. J. Savory, "Blind Equalization and Carrier Phase Recovery in a 16-QAM Optical Coherent System," *J. Lightw. Technol.,* vol. 27, no. 15, pp. 3042-3049, 2009.

[57] K. P. Zhong, J. H. Ke, Y. Gao, J. C. Cartledge, A. P. T. Lau and C. Lu, "Carrier Phase Estimation for DP-16QAM using QPSK Partitioning and Quasi-multiplier-free algorithms," in *OFC,* 2014.

[58] M. Seimetz, "Laser Linewidth limitations for optical systems with high-order modulation employing feed forward digital carrier phase estimation," in *OFC*, 2008.

[59] T. Pfau, S. Hoffmann and R. Noe, "Hardware-efficient cohrerent digital receiver concept with feedforward carrier recovery for M-QAM constellations," *JLT,* vol. 27, no. 8, pp. 989-999, 2009.

[60] S. M. Bilal, etal., "Low-Complexity.linewidth-tolerant carrier phase estimation for 64-QAM systems based on constellation transformation," in *ECOC*, 2013.

[61] X. Zhou, "An Improved Feed-Forward Carrier Recovery Algortihm for Coherent Receivers with M-QAM Modulations Format," *IEEE Photon. Technol. Lett.,* vol. 22, no. 14, pp. 1051-1053, 2010.

[62] Yang, Hui, etal., "SUDOI: software defined networking for ubiquitous data center optical interconnection," *IEEE Communications Magazaine,* vol. 54, no. 2, pp. 86-95, 2016.

[63] O. Gerstel, M. Jinno, A. Lord and S. J. Yoo, "Elastic Optical Networking: A new dawn for the optical layer?," *IEEE Commun. Mag.,* vol. 50, no. 2, pp. s12-s20, 2012.

[64] M. Angelou, etal., "Spectrum, cost and energy efficiency in fixed-grid and flex-grid networks," in *OFC/NOFEC*, 2012.

[65] R. A. Soriano, F. N. Hauske, N. G. Gonzalez, Z. Zhang, Y. Ye and I. T. Monroy, "Chromatic dispersion estimation in digital coherent receivers," *J. Lightw. Technol.,* vol. 29, no. 11, pp. 1627-1637, 2011.

[66] Q. Sui, A. P. T. Lau and C. Lu, "Fast and Robust Blind Chromatic Dispersion Estimation Using Auto-Corrrection of Signal Power Waveform for Digital Coherent Systems," *JLT*, vol. 31, no. 2, pp. 306-312, 2013.

[67] T. Nagakawa, M. Matsui, T. Kobayashi, K. Ishihara, R. Kudo, M. Mizoguchi and Y. Miyamoto, "Non-Data-Aided Wide-Range Frequency Offset Estimator for QAM Optical Coherent Receivers," in *OFC*, 2011.

[68] X. Zhou, K. Zhong, Y. Gao, C. Lu, A. P. T. Lau and K. Long, "Modulation-format-independent blind phase search algorithm for coherent optical square M-QAM systems," *Optics Express,* vol. 22, no. 20, pp. 24044-24054, 2014.

[69] Y. G. A. P. T. Lau and C. Lu, "Modulation-format-independent carrier phase estimationtechnique for square M-QAM systems," *IEEE Photon. Technol. Lett.,* vol. 25, no. 11, pp. 1073-1076, 2013.

[70] J. Zhang, J. Yu, B. Zhu, F. Li, H. -C. Chien, Z. Jia, Y. Cai, X. Li, X. Xiao, Y. Fang and Y. Wang, "Transmission of single-carrier 400G signals (515.2-Gb/s) based on 128.8-GBaud PDM QPSK over 10130- and 6078 km terrestrial fiber links," *Optics Express,* vol. 23, no. 13, pp. 16540-16545, 2015.

[71] G. Raybon, etal., "Single-carrier all-ETDM 1.08-Terabit/s line rate PDM-64-QAM transmitter using a high-speed 3-bit multiplexing DAC," in *IEEE Photonics Conference (IPC)*, 2015.

[72] H. Mardoyan, etal., "Transmission of single-carrier Nyquist-shaped 1-Tb/s line-rate signal over 3000 km," in *OFC*, 2015.

[73] B. Guan, etal., "Bandwidth scalable and high fidelity spectrally-sliced transmitter," in *OFC*, 2015.

[74] Thorlabs, "Pigtailed External Cavity (ECL) Single-Frequency Lasers, Butterfly Package," Thorlabs, 2017. [Online]. Available: https://www.thorlabs.com/newgrouppage9.cfm?objectgroup_id=4934. [Accessed 11 June 2017].